POLITECNICO DI TORINO
Repository ISTITUZIONALE

Cell orientation under stretch: Stability of a linear viscoelastic model

(Article begins on next page)

05 May 2024

Cell Orientation under Stretch: Stability of a Linear Viscoelastic Model

Giulio Lucci *†‡   Chiara Giverso *   Luigi Preziosi *

May 10, 2021

Abstract

The sensitivity of cells to alterations in the microenvironment and in particular to external mechanical stimuli is significant in many biological and physiological circumstances. In this regard, experimental assays demonstrated that, when a monolayer of cells cultured on an elastic substrate is subject to an external cyclic stretch with a sufficiently high frequency, a reorganization of actin stress fibers and focal adhesions happens in order to reach a stable equilibrium orientation, characterized by a precise angle between the cell major axis and the largest strain direction. To examine the frequency effect on the orientation dynamics, we propose a linear viscoelastic model that describes the coupled evolution of the cellular stress and the orientation angle. We find that cell orientation oscillates tending to an angle that is predicted by the minimization of a very general orthotropic elastic energy, as confirmed by a bifurcation analysis. Moreover, simulations show that the speed of convergence towards the predicted equilibrium orientation presents a changeover related to the viscous-elastic transition for viscoelastic materials. In particular, when the imposed oscillation period is lower than the characteristic turnover rate of the cytoskeleton and of adhesion molecules such as integrins, reorientation is significantly faster.

Keywords: Cell orientation · Cell stretching · Stress fibers · Cell mechanosensing · Viscoelasticity · Bifurcations

2020 Mathematics Subject Classification: 74D05 · 74L15 · 92C10 · 92C37

1   Introduction

During their life cycle, cells are constantly exposed to numerous stimuli coming from the surrounding microenvironment. The nature of these cues is wide-ranging: among them, a significant role is played by mechanical prompts, since many experiments demonstrated that they trigger a cellular response [1, 6, 9, 15, 22, 29, 33, 47, 65, 74]. Cell sensitivity to mechanical actions is relevant in many biological and physiological circumstances, such as growth, differentiation,

---

*Department of Mathematical Sciences "G.L. Lagrange" Dipartimento di Eccellenza 2018-2022, Politecnico di Torino, Corso Duca degli Abruzzi 24, 10129 Turin, Italy

†Department of Mathematics "G. Peano", Università degli Studi di Torino, Via Carlo Alberto 10, 10123 Turin, Italy

‡Corresponding author. E-Mail address: `giulio.lucci@polito.it`

motility, apoptosis and tissue fibrosis [7, 29, 65]. Its precise understanding has then gathered increasing research attention, since it could be helpful to acquire a deeper knowledge of some diseases and of morphogenesis, just to mention a few examples. For instance, an altered perception of mechanical stimuli due to cell-cell contact inhibition and to cell tensile stress is known to have a role in tumourigenesis and cancer development [5, 8, 32, 36], and it is also related to epithelial-mesenchymal transition [31, 58] in neoplastic tissues.

Moreover, the active response of the cell to mechanical interactions with the environment is involved in cell culturing, development, and tissue engineering. In particular, during embryogenesis, the formation of residual stresses and active forces is believed to drive heart formation and looping [60]. Cardiac cell cultures also display enhanced hypertrophy, proliferation and alignment when subject to static or cyclic stress [64]. Notably, experimental tests carried out on several types of cells (like fibroblasts, myofibroblasts, cardiomyocites and endothelial cells) showed that alignment in response to a deformation is a common feature which proves their capability to adapt after mechanical stimuli [1, 9, 15, 40, 46, 47, 48]. In detail, when a monolayer undergoes a cyclic deformation, cells lying on the substrate tend to change their orientation in a precise way, until they reach a stable configuration characterized by a well-defined angle between their major axis and the direction of largest stretching. In this process, a fundamental role is played by the cytoskeleton [27, 47, 66, 67]: focal adhesions (FAs), i.e. protein complexes which provide cell contact with the substrate and the extracellular matrix, sense the mechanical stress and induce a remodelling of the cytoskeletal structure, through the formation of oriented actin stress fibers (SFs). These fiber bundles are able to develop contractile forces: when submitted to an external stretch, the cell reorganizes the SF structure, disrupting and rebuilding them in a specific direction to relieve the stress.

Several works, both on the experimental [1, 11, 15, 23, 27, 30, 33, 40, 47, 68] and on the theoretical side [3, 9, 17, 18, 19, 67, 70], have tried to address the problem of cell reorientation under mechanical stretch. It is recognized that this mechanism is actively performed by the cell [69], and that it is induced by mechanical strain deforming the substrate to which they adhere. Moreover, there is common agreement on the fact that cells on a plane substrate undergoing a cyclic deformation orient their stress fibers in a direction which is oblique or in some cases perpendicular to the applied strain [9, 27, 40, 45]. Indeed, when the substrate deformation is transmitted to the cell cytoskeleton through FAs, a reorganization of SF structure happens: they are disassembled and rebuilt in a precise direction [56], fostering changes in shape and orientation of the whole cell. In addition, FAs themselves form clusters at the ends of aligned SFs, giving the cell an elongated and clearly oriented morphology (see Fig.1). Therefore it is possible to define an equilibrium *orientation angle*, θ_{eq}, that is the angle formed by the cell major axis and the direction of stretching when cell orientation does not evolve anymore. In this respect, mathematical models trying to predict this equilibrium orientation angle and the driving force of such a behaviour have been proposed, using different approaches but mainly in a linear elastic framework. For instance, the first attempts to describe cell orientation suggested a preference for the minimal strain or minimal stress directions [18, 19, 23, 40, 66, 68]. Looking closely at biaxial tests, Livne and coworkers [40] found a linear relationship between $\cos^2 \theta_{eq}$ and a parameter quantifying the biaxiality of the deformation.

Remarkably, some experimental assays were performed applying deformations for which using linear elasticity should be theoretically inaccurate (e.g., up to 24% in [40] and up to 32% in [23]). Starting from this experimental evidence, Lucci and Preziosi [42] proved that a generalization of the linear relationship found in the linear elastic case by Livne et al. [40] also holds for a very large class of nonlinear constitutive orthotropic models. In the nonlinear framework, the squared cosine of the orientation angle is linearly dependent on a parameter which is the natural generalization of the one found in [40], with a slope depending on a combination of elastic
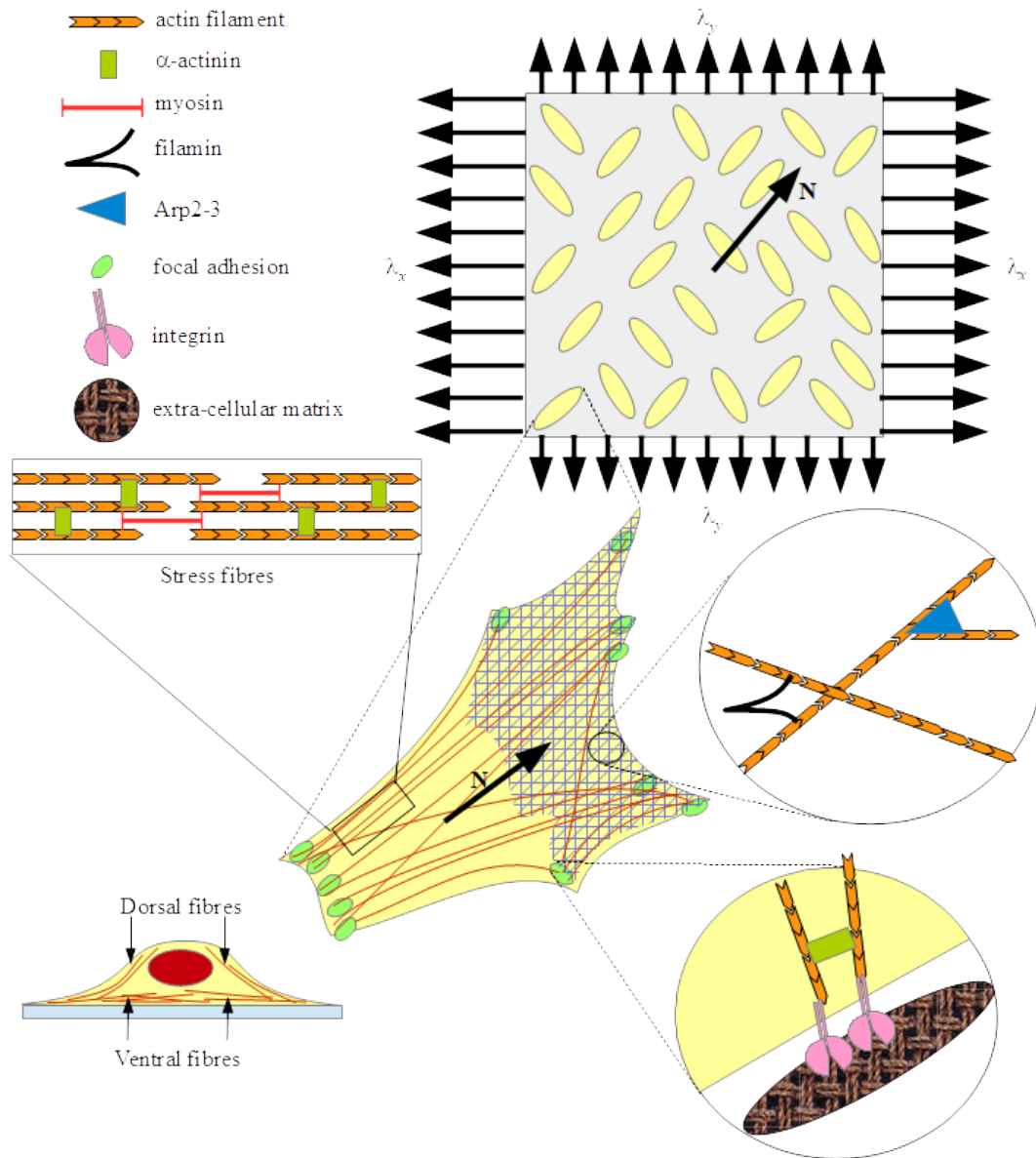
Figure 1: Sketch of experimental set-up, of the inner structure of a typical cell, and of its adhesion to the substrate.

coefficients characterizing the nonlinear strain energy.

Nevertheless, there are other factors influencing the orientation of the cell, the most relevant of which is probably the frequency of the applied cyclic deformation [30, 38]. In fact, it has been observed that, in order to trigger such a response, the period of the stretching cycle must be sufficiently small [28, 30]. As specified in [30], this threshold seems to be cell-type dependent, leading to minimum frequencies that go from 0.01 Hz for rat embryonic fibroblasts to 0.1 Hz for human dermal fibroblasts. This mechanism cannot be covered by the purely elastic descriptions discussed above, and calls for the introduction of a characteristic response time that needs to be compared with the periodic deformation time scale. The existence of such a characteristic time might be related to the reorganization of the acto-myosin cytoskeleton and of the ensemble of focal adhesions with the substrate. Indeed, it is known that the characteristic turnover times of both phenomena are of the order of tens of seconds, or even minutes (see, for instance, [11, 50, 51, 63]).

On the basis of this observation, in this paper we propose a viscoelastic model for cell preferential orientations, in order to describe reorganization processes occurring inside the cell and between the cell and its microenvironment when a mechanical deformation is applied to the substrate. To our knowledge, previous viscoelastic descriptions of cell stress fiber dynamics have been mainly focused on the microscopic scale [35, 55], while in this article we treat the monolayer as a continuum. In particular, we introduce an anisotropic viscoelastic description that couples the evolution of the SF orientation angle with the mechanical stress exerted on the cell as a consequence of cyclic stretching. Hence, the ensemble of cells lying on the substrate is considered as a Maxwell orthotropic fluid with a single relaxation time. We prove that, for high stretching frequencies, the cell cytoskeleton does not have enough time to reorganize and behaves elastically, while for slow processes the viscous character emerges.

Futhermore, after having showed that the steady angles are predicted by an energy minimization, we work with a very general orthotropic material. An extensive bifurcation analysis is then performed, discussing the role of elastic parameters and finding the conditions under which a certain angle of cell orientation is stable. We find that also in this general set up there exists a linear relationship between $\cos^2 \theta_{eq}$ and a combination of parameters of the orthotropic elasticity tensor. The slope of the straight line fitting experimental data suggests that, among all coefficients, a more relevant role is played by those in charge of describing the cell response to elongation along its orientation axis and to shear.

Finally, we perform some numerical simulations using the complete viscoelastic model, studying the reorientation dynamics in the high frequency and low frequency cases together with stress evolution. It is found that the cell orientation angle evolves toward the steady state predicted by the linear stability analysis, with a speed which depends on the elastic or viscous character of the system. Moreover, in accordance with the observation in [28, 30], simulations show that the speed of reorientation towards the equilibrium angle sensibly depends on the frequency of imposed oscillations. In particular, it presents a transition for values of the ratio of the oscillation period and the characteristic time of viscoelasticity close to 2π, so that the time required to observe reorientation is of the order of days for smaller frequencies, saturating to one hour for larger frequencies.

In detail, the paper is organized as follows. In Section 2 the general mathematical model is introduced, deriving the equations for the viscoelastic system and studying their significant limits, i.e. the high-frequency and low-frequency cases. Section 3 is devoted to a detailed bifurcation analysis of the model for an orthotropic energy density, deriving conditions under which equilibrium orientations are stable. In Section 4 we discuss the implementation and report some numerical results of our model, showing both the elastic and the viscous behaviour of the system. Finally, Section 5 is dedicated to a summary of the results and to the discussion of some open issues, which may be of interest for future research. In Appendix A we report some details

4

related to the possible presence of a symmetry breaking phenomenon.

2 Viscoelastic Model

We consider a two-dimensional substrate seeded of cells that is stretched biaxially. While the response of the extracellular material is in general isotropic and elastic, the mechanical behaviour of the ensemble of cells can be regarded as anisotropic and viscoelastic. The viscoelastic character is due to the reorganization of the acto-myosin network inside the cell and to the rearrangement of focal adhesions (FAs), performed through repeated detachments and attachments of integrin bonds with the substrate, especially under stretch, to relax the perceived stress (see, for instance, [54]). Instead, anisotropy derives from the fact that, when subject to a mechanical deformation, cells tend to build properly oriented actin stress fibers (SFs) within their cytoskeleton [29, 66]. In addition, these SFs are linked by a network of proteins (such as fascin, fimbrin, α-actinin, filamin, ARP2-3 [14, 24, 57, 67]) that spans them orthogonally with respect to the fiber bundles or at well defined angles, as in the case or ARP2-3, as sketched in Fig. 1. As a consequence, the cell responds differently to stretches and stresses along its major axis with respect to the transversal axis and to shear as well.

The main orientation of SFs, which will be identified by a unit vector $\mathbf{N}$, can change in time due to several cues, among which mechanical deformations. We will here consider, as in experiments, that the specimen is subject to a biaxial stretch and take the x-axis aligned to the direction of maximal stretch. Then, the angle formed by $\mathbf{N}$ and the x-axis will be denoted by θ.

Resorting to Lagrangian mechanics, we can relate the evolution in time of the orientation angle θ with the changes in the virtual work $\mathcal{L}$ done by the stress acting on the cell due to SF alignment. Considering an overdamped regime, which corresponds to neglecting inertial effects, we can then write

$$0 = -\eta \frac{d\theta}{dt} - \frac{\partial \mathcal{L}}{\partial \theta} \,, \tag{1}$$

where $\mathcal{L} := \mathbb{T} : \mathbb{E}$, being $\mathbb{T}$ the excess Cauchy stress tensor and $\mathbb{E}$ the infinitesimal deformation tensor, is the work done by the stress, assuming that the mechanical behaviour is linear. Moreover, $\eta > 0$ is a viscous-like coefficient measuring cell resistance to realignment. Since we are interested in deformation tests, where a periodic deformation is imposed to the specimen, $\mathbb{E}$ is assumed to be independent of θ and externally imposed. It is then convenient to rearrange Eq. (1) to get the following evolution equation for $\theta(t)$:

$$\frac{d\theta}{dt}(t) = -\frac{1}{K\lambda_\theta} \frac{\partial \mathbb{T}}{\partial \theta}(t|\theta) : \mathbb{E}(t) \,, \tag{2}$$

where we identified K as the characteristic Young modulus of the material and $\lambda_\theta := \eta/K$ as a parameter related to the time the cell takes to reorient itself. The notation $\mathbb{T}(t|\theta)$ reads as the stress at time t given the history of orientations θ.

Equation (2) implies that, for a given deformation $\mathbb{E}$, θ tends to assume a value such that the variation of $\mathbb{T}$ with respect to θ either vanishes or becomes orthogonal to $\mathbb{E}$.

Focusing on $\mathbb{T}$, we assume here that the stress in the elastic substrate and the viscoelastic cellular component embedded in it is given by

$$\mathbb{T}(t|\theta) = \int_{-\infty}^{t} \mathbb{C}(\theta(\tau); t - \tau)[\mathbb{E}(t) - \mathbb{E}(\tau)] \, d\tau \,, \tag{3}$$

(see, for instance, [2] for the isotropic case and [52, 53] for the anisotropic case). We notice that the elements of the fourth-order tensor $\mathbb{C}$ are all bounded and that, in the isotropic case,

$\mathbb{C}$ reduces to the derivative of the so-called relaxation kernel (apart from the sign) times the identity tensor. The kernel $\mathbb{C}$ depends on the alignment direction, i.e. on the orientation angle θ, which during the history of deformation can evolve in time. On the other hand, the second part of the kernel dependence takes into account the weight of past orientations (at time τ) on the present state of stress and represents memory effects of the viscoelastic material. We will assume that such a dependence is exponential with a single relaxation time λ [52, 53], that is,

$$\mathbb{C}(\theta(\tau); t - \tau) = \frac{1}{\lambda}\mathbb{C}_0(\theta(\tau))e^{-(t-\tau)/\lambda}, \tag{4}$$

where $\mathbb{C}_0(\theta(\tau))$, which is the fourth-order elasticity tensor depending on the orientation direction θ at time τ, inherits form $\mathbb{C}$ the boundedness and regularity properties. Therefore, we can write

$$\mathbb{T}(t|\theta) = \int_{-\infty}^{t} \frac{1}{\lambda}e^{-(t-\tau)/\lambda}\mathbb{C}_0(\theta(\tau))[\mathbb{E}(t) - \mathbb{E}(\tau)]\,d\tau\,. \tag{5}$$

As usual in rheology, for this type of kernels it is useful to differentiate (5) and to rewrite the constitutive equation in the following differential form:

$$\lambda\frac{d\mathbb{T}}{dt}(t|\theta) + \mathbb{T}(t|\theta) = \mathbb{\mathbb{C}}_0(t|\theta)\frac{d\mathbb{E}}{dt}(t)\,, \tag{6}$$

where

$$\mathbb{\mathbb{C}}_0(t|\theta) := \int_{-\infty}^{t} e^{-(t-\tau)/\lambda}\mathbb{C}_0(\theta(\tau))\,d\tau = \int_{0}^{+\infty} \lambda e^{-s}\mathbb{C}_0(\theta(t-\lambda s))\,ds\,, \tag{7}$$

is a functional on the exponentially weighted history of past orientations. We observe that, in the isotropic case, $\mathbb{\mathbb{C}}_0$ is twice the so-called elastic viscosity, i.e., the area under the relaxation kernel (times the identity tensor).

In Eq. (2) and (6) there are two intrinsic characteristic times: λ refers to the viscous behaviour of cells due, for instance, to the continuous renewal of adhesion bonds with the substrate, while λ_θ is related to the characteristic time of reorganization of stress fibers and consequently to the change in cell orientation. It is known that both remodelling phenomena occur on time scales of tens of seconds or even minutes [11, 50, 51, 63]. Now, given that in mechanical tests cells are often subject to cyclic strains, it is useful to discuss how the model behaves when the imposed oscillation period T is much shorter or longer than the characteristic times mentioned above. In order to do so, we observe that, for a periodic deformation $\mathbb{E}(t) = \mathbb{E}_0 e^{i\omega t}$, the expression of the stress (5) can be rewritten as

$$\mathbb{T}(t|\theta) = \frac{1}{\lambda}\left[\int_{-\infty}^{t} e^{-(t-\tau)/\lambda}\,\mathbb{C}_0(\theta(\tau))\left(1 - e^{-i\omega(t-\tau)/\lambda}\right)\,d\tau\right]\mathbb{E}_0 e^{i\omega t}$$

$$= \left[\int_{0}^{+\infty} e^{-s}\,\mathbb{C}_0(\theta(t-\lambda s))\left(1 - e^{-i\lambda\omega s}\right)\,ds\right]\mathbb{E}_0 e^{i\omega t}\,. \tag{8}$$

2.1 High Frequency Regime

First of all, we consider a high frequency regime with $\lambda, \lambda_\theta \gg T = 2\pi/\omega$, so that the relaxation times are much longer than the oscillation period of the deformation, i.e., the reorganization

process is slower than the imposed cyclic strain. In this case, it is useful to split the integral in Eq. (8) as

$$\mathbb{T}(t|\theta) = \left[\int_0^{+\infty} e^{-s} \mathbf{C}_0(\theta(t-\lambda s))\, ds \right] \mathbb{E}_0 e^{i\omega t} - \left[\int_0^{+\infty} e^{-s} \mathbf{C}_0(\theta(t-\lambda s)) e^{-i\lambda\omega s}\, ds \right] \mathbb{E}_0 e^{i\omega t}. \quad (9)$$

We observe that, as stated before, the coefficients of tensor $\mathbf{C}_0(\theta(t))$ are regular in θ. In particular, they are bounded as well as their derivatives. Hence, by Riemann-Lebesgue lemma, the second integral in the r.h.s. of Eq. (9), which can be regarded as the unilateral Fourier transform of the L^1 function $e^{-s}\mathbf{C}_0(\theta(t-\lambda s))$, vanishes in the limit of high frequencies.

As regards the first term, integrating by parts and exploiting Eq. (2) we have

$$\mathbb{T}(t|\theta) = \left[\mathbf{C}_0(\theta(t)) + \frac{\lambda}{K\lambda_\theta} \int_0^{+\infty} e^{-s} \frac{\partial\mathbf{C}_0}{\partial\theta}(\theta(t-\lambda s)) \frac{\partial\mathbb{T}}{\partial\theta}(t-\lambda s|\theta) : \mathbb{E}_0 e^{i\omega(t-\lambda s)}\, ds \right] \mathbb{E}_0 e^{i\omega t}$$

$$= \mathbf{C}_0(\theta(t))\mathbb{E}_0 e^{i\omega t} + \left[\frac{\lambda}{K\lambda_\theta} \int_0^{+\infty} e^{-s} \frac{\partial\mathbf{C}_0}{\partial\theta}(\theta(t-\lambda s)) \frac{\partial\mathbb{T}}{\partial\theta}(t-\lambda s|\theta) : \mathbb{E}_0 e^{-i\lambda\omega s}\, ds \right] \mathbb{E}_0 e^{i2\omega t}.$$

Provided that, denoting by $H(s)$ the Heaviside function, the tensorial function

$$\mathbf{f}(s) = H(s) \frac{\partial\mathbf{C}_0}{\partial\theta}(\theta(t-\lambda s)) \frac{\partial\mathbb{T}}{\partial\theta}(t-\lambda s|\theta) : \mathbb{E}_0 e^{-s} \quad \in L^1(\mathbb{R}),$$

as we expect because of the boundedness of the derivative of the coefficients in $\mathbf{C}_0$, the integral in the stress expression corresponds to the Fourier transform of $\mathbf{f}(s)$, which again vanishes in the limit of high frequencies. Hence, in the high frequency regime we are left with

$$\mathbb{T}(t|\theta) \approx \mathbf{C}_0(\theta(t))\mathbb{E}_0 e^{i\omega t}. \quad (10)$$

Such a constitutive equation corresponds to an anisotropic linear elastic response of the material, where $\mathbf{C}_0(\theta(t))$ is the fourth-order elasticity tensor depending on the orientation θ.

So, in the high frequency regime Eq. (2) can be simplified to

$$\frac{d\theta}{dt} = -\frac{1}{\eta}\left[\frac{\partial\mathbf{C}_0}{\partial\theta}\mathbb{E} \right] : \mathbb{E} = -\frac{2}{K\lambda_\theta}\frac{\partial U}{\partial\theta}, \quad (11)$$

where

$$U(t,\theta) := \frac{1}{2}\mathbb{E}(t) : \mathbf{C}_0(\theta)\mathbb{E}(t), \quad (12)$$

is the elastic strain energy. Therefore, in the high frequency regime, the change in cell orientation is driven by the minimization of an elastic energy with respect to the orientation angle, coherently with previous models and experimental results [40, 42].

2.2 Low Frequency Regime

In a low frequency regime, in which the period of the cyclic strain imposed to the specimen is much longer than the characteristic time λ of cell relaxation, the reorientation process is faster than the external oscillations. Therefore, taking into account the approximation $\lambda \ll T = 2\pi/\omega$, or equivalently $\lambda\omega \ll 1$, we have that

$$1 - e^{-i\lambda\omega s} \approx i\lambda\omega s,$$

7

and the stress can be expressed using Eq. (8) through

$$\mathbb{T}(t|\theta) \approx i\lambda\omega \left[\int_0^{+\infty} se^{-s}\mathbb{C}_0(\theta(t-\lambda s))\, ds \right] \mathbb{E}_0 e^{i\omega t},$$ (13)

which, defining

$$\overline{\mathbb{C}}_0(t|\theta) := \int_0^{+\infty} se^{-s}\mathbb{C}_0(\theta(t-\lambda s))\, ds,$$

shows an anisotropic viscous-like response characterized by the constitutive equation

$$\mathbb{T}(t|\theta) \approx \lambda\overline{\mathbb{C}}_0(t|\theta)\frac{d\mathbb{E}}{dt}(t).$$ (14)

Essentially, if the imposed oscillations are sufficiently slow, the system behaviour is similar to the one of a viscous fluid with anisotropy induced by oriented cells. Moreover, since we are mostly interested in steady orientations, given that $\mathbb{C}_0(\theta(t-\lambda s))$ is an analytic function on $\mathbb{R}$ it is possible to write

$$\mathbb{C}_0(\theta(t-\lambda s)) = \mathbb{C}_0(\theta(t)) + \mathbb{C}_0'(\theta(t))\frac{d\theta}{dt}(t)(-\lambda s)$$

$$+ \frac{1}{2}\left[\mathbb{C}_0''(\theta(t))\left(\frac{d\theta}{dt}(t)\right)^2 + \mathbb{C}_0'(\theta(t))\frac{d^2\theta}{dt^2}(t) \right](-\lambda s)^2 + \dots$$

and therefore, at the equilibrium orientations,

$$\mathbb{C}_0(\theta(t-\lambda s)) \approx \mathbb{C}_0(\theta(t)).$$ (15)

By means of this approximation, we can write the steady state oscillatory stress in the low frequency regime using Eq. (14) and Eq. (15) as

$$\mathbb{T}(t|\theta) \approx \lambda\mathbb{C}_0(\theta(t))\frac{d\mathbb{E}}{dt}(t).$$ (16)

Comparing the latter with the stress in the high frequency case (10), we observe that they essentially differ for a factor $\lambda\omega$, as will be highlighted in the simulations.

Finally, recalling Eq. (2), we have that the angle θ tends to assume, as already stated, the configuration such that $\frac{\partial \mathbb{T}}{\partial \theta} \perp \mathbb{E}$, which in the low frequency limit writes as

$$\left(\frac{\partial \mathbb{C}_0}{\partial \theta}\frac{d\mathbb{E}}{dt} \right) \perp \mathbb{E}.$$

However, since the deformation is periodic, the last condition can be rephrased as

$$i\omega \left(\frac{\partial \mathbb{C}_0}{\partial \theta}\mathbb{E}_0 \right) : \mathbb{E}_0 = 0 \qquad \implies \qquad \frac{\partial U}{\partial \theta} = 0,$$

where U is the elastic energy defined in (12). Therefore, we conclude that in the low frequency regime also in the viscoelastic case the steady cell configurations are predicted by a minimization with respect to the orientation angle θ of the energy introduced in the elastic case.

We remark that, even though our model predicts that the equilibrium orientation of the cell is the same in both regimes, the characteristic time of reorientation is highly influenced by the frequency, leading therefore to different final orientation angles of the cell in the two regimes, considering the time of the biological experiment, as will be shown in Section 4.

3 Bifurcation Analysis

In this Section, we study equilibrium orientations and their bifurcations. Our goal is to describe the monolayer subject to a periodic stretch through its elastic energy, since the steady orientation of the cells is predicted by its minimization as discussed above. This allows us to study in detail the equilibrium angles in terms of a very general strain energy, looking for those orientations which minimize it for a fixed deformation. Finally, we draw bifurcation diagrams in terms of a parameter that quantifies the biaxiality of the deformation, putting in evidence the conditions under which the preferential orientations exist and are stable. This is in agreement with previous works showing that an energetic approach allows to reproduce experimental data of cell orientation more accurately [40].

3.1 Elastic Energy and Deformation

We consider the most general elastic energy density U depending on the classical first three invariants $I_1 := \text{tr}\,\mathbb{C}$, $I_2 := \frac{1}{2}\left[(\text{tr}\,\mathbb{C})^2 - \text{tr}\,\mathbb{C}^2\right]$ and $I_3 := \det \mathbb{C}$ (where $\mathbb{C} = \mathbb{F}^T \mathbb{F}$ is the right Cauchy-Green deformation tensor and $\mathbb{F}$ is the deformation gradient) representing the isotropic response of the material, and on the anisotropic invariants [49]

$$I_4 := \mathbf{N} \cdot \mathbb{C}\mathbf{N} = |\mathbb{F}\mathbf{N}|^2, \qquad I_5 := \mathbf{N} \cdot \mathbb{C}^2\mathbf{N} = |\mathbb{C}\mathbf{N}|^2,$$

$$I_6 := \mathbf{N}_\perp \cdot \mathbb{C}\mathbf{N}_\perp = |\mathbb{F}\mathbf{N}_\perp|^2, \qquad I_7 := \mathbf{N}_\perp \cdot \mathbb{C}^2\mathbf{N}_\perp = |\mathbb{C}\mathbf{N}_\perp|^2, \tag{17}$$

$$I_8 := \mathbf{N}_\perp \cdot \mathbb{C}\mathbf{N} = (\mathbb{F}\mathbf{N}_\perp) \cdot \mathbb{F}\mathbf{N}\,.$$

Then, the general energy functional can be written as

$$U = U_i(I_1, I_2, I_3) + U_\ell(I_1, I_2, I_3, I_4, I_5, I_6, I_7, I_8) + U_q(I_4, I_5, I_6, I_7, I_8), \tag{18}$$

where U_i is the purely isotropic contribution, U_q is the purely anisotropic one and U_ℓ includes a coupling between isotropic and anisotropic terms. However, since the invariants I_1, I_2, I_3 do not depend on the orientation angle, the inclusion of U_i will not influence the following discussion. Henceforth, the energy dependence upon it will not be explicitly mentioned anymore, though one should recall that this term might appear in an irrelevant way as an extra contribution in the energy that does not alter our results and conclusions.

Considering the limit of small deformations and denoting by $\mathbb{E}$ the infinitesimal strain tensor, one has

$$I_4 \approx 1 + 2\mathbf{N} \cdot \mathbb{E}\mathbf{N}\,, \qquad I_5 \approx 1 + 4\mathbf{N} \cdot \mathbb{E}\mathbf{N}\,,$$

$$I_6 \approx 1 + 2\mathbf{N}_\perp \cdot \mathbb{E}\mathbf{N}_\perp\,, \quad I_7 \approx 1 + 4\mathbf{N}_\perp \cdot \mathbb{E}\mathbf{N}_\perp\,,$$

$$I_8 \approx 2\mathbf{N}_\perp \cdot \mathbb{E}\mathbf{N},$$

so that in linear elasticity it is impossibile to discriminate the dependence on I_4 (resp. I_6) from the one on I_5 (resp. I_7), since they both merge in a dependence on $\mathbf{N} \cdot \mathbb{E}\mathbf{N}$ (resp. $\mathbf{N}_\perp \cdot \mathbb{E}\mathbf{N}_\perp$). As a consequence, working in a linear framework, from now on we will consider the following dependences:

$$U_q = U_q\left(\hat{I}_4, \hat{I}_6, I_8\right) \quad \text{and} \quad U_\ell = U_\ell\left(\hat{I}_i\hat{I}_4, \hat{I}_i\hat{I}_6, \hat{I}_i I_8\right), \quad i = 1, 2, 3,$$

where we have defined

$$\hat{I}_1 := I_1 - 2, \qquad \hat{I}_2 := I_2 - 2, \qquad \hat{I}_3 := I_3 - 1,$$

$$\hat{I}_4 := I_4 - 1 \propto \mathbf{N} \cdot \mathbb{E}\mathbf{N}, \quad \hat{I}_6 := I_6 - 1 \propto \mathbf{N}_\perp \cdot \mathbb{E}\mathbf{N}_\perp. \tag{19}$$

Consider now a biaxial extension experiment. We assume that the deformation inside the specimen is homogeneous, so that in two dimensions the deformation gradient reads

$$\mathbb{F} = \begin{pmatrix} \lambda_x & 0 \\ 0 & \lambda_y \end{pmatrix},$$

where we take $\lambda_x > \lambda_y$ since in our notation, as stated before, the maximum stretching is performed along the x-direction. For future comparison we will denote $\lambda_x = 1+\varepsilon$ and $\lambda_y = 1-r\varepsilon$, so that for small ε - i.e. for small deformations - the infinitesimal strain tensor writes

$$\mathbb{E} = \begin{pmatrix} \varepsilon & 0 \\ 0 & -r\varepsilon \end{pmatrix}, \tag{20}$$

where the parameter r is often referred to as the *biaxiality ratio*. We also observe that the assumption $\lambda_x > \lambda_y$ implies $r + 1 > 0$. Finally, we remark that the particular case $\lambda_x = \lambda_y$, corresponding to $r = -1$, will not be discussed explicitly and is not really interesting from the practical point of view as experimental evidence showed that, under equi-biaxial stretch, cells do not orient in a specific direction in the plane of the deformation [67].

Recalling that θ is the angle formed by the average cell orientation direction and the x-axis, then $\mathbf{N} = (\cos\theta, \sin\theta)$ and one has

$$\mathbf{N} \cdot \mathbb{E}\mathbf{N} = (\cos^2\theta - r\sin^2\theta)\varepsilon = [(r+1)\cos^2\theta - r]\varepsilon\,,$$

$$\mathbf{N}_\perp \cdot \mathbb{E}\mathbf{N}_\perp = [1 - (r+1)\cos^2\theta]\varepsilon\,,$$

$$\mathbf{N}_\perp \cdot \mathbb{E}\mathbf{N} = -(r+1)\sin\theta\cos\theta\,\varepsilon\,,$$

and therefore, in the small deformation approximation, we can write both terms U_ℓ and U_q of the elastic energy as functions of θ.

As regards U_q, the most general elastic constitutive model for linear elasticity takes the following quadratic form:

$$U_q\left(\hat{I}_4, \hat{I}_6, I_8\right) = \frac{1}{2}K_\parallel(\mathbf{N} \cdot \mathbb{E}\mathbf{N})^2 + \frac{1}{2}K_\perp(\mathbf{N}_\perp \cdot \mathbb{E}\mathbf{N}_\perp)^2 + \frac{1}{2}K_s(\mathbf{N}_\perp \cdot \mathbb{E}\mathbf{N})^2$$

$$+ K_{\parallel\perp}(\mathbf{N} \cdot \mathbb{E}\mathbf{N})(\mathbf{N}_\perp \cdot \mathbb{E}\mathbf{N}_\perp) + K_{\parallel s}(\mathbf{N} \cdot \mathbb{E}\mathbf{N})(\mathbf{N}_\perp \cdot \mathbb{E}\mathbf{N}) + K_{\perp s}(\mathbf{N}_\perp \cdot \mathbb{E}\mathbf{N}_\perp)(\mathbf{N}_\perp \cdot \mathbb{E}\mathbf{N})\,, \tag{21}$$

where $K_\parallel$ is a coefficient related to the stiffness to stretching in the direction of cell orientation, $K_\perp$ to the one in the orthogonal direction, and K_s to the one related to shear. The other coefficients are due to mixing effects among these three. We remark that the coefficient K_s weights the response to shear: then, at the microsopic level, it quantifies the resistance to a change in angle between stress fibers, which also involves the cross-linking network of proteins like filamin, Rho/Rac GTPases, and ARP2/3 mentioned above.

In terms of θ, the anisotropic part of the energy can then be written as

$$U_q(\theta) = \frac{1}{2}\varepsilon^2\Big\{ K_\parallel[\xi(\theta) - r]^2 + K_\perp[1 - \xi(\theta)]^2 + K_s\,\xi(\theta)[r + 1 - \xi(\theta)]$$

$$+ 2K_{\parallel\perp}[\xi(\theta) - r][1 - \xi(\theta)] - 2K_{\parallel s}[\xi(\theta) - r](r+1)\sin\theta\cos\theta$$

$$-2K_{\perp s}[1-\xi(\theta)](r+1)\sin\theta\cos\theta\Big\}, \tag{22}$$

where $\xi(\theta) := (r+1)\cos^2\theta$. We remark that, here and in the remainder of this Section, we have dropped the explicit energy dependence on t, since we are interested in the steady orientations of the cells which do not depend on time.

Moreover, we point out that, in the following, we will take $K_{\parallel s} = K_{\perp s} = 0$ due to symmetry requirements on the energy. Indeed, for the problem at hand, biological observations suggest that the energy must be symmetric with respect to $\theta = 0$ and $\theta = \pi/2$, that is,

$$U(-\theta) = U(\pi - \theta) = U(\theta) \qquad \forall\,\theta\,.$$

These symmetries are biologically reasonable and not surprising: in absence of other directional stimuli, there is no reason why the cell should prefer the configuration $-\theta$ instead of the one characterized by the angle θ, as well as $\pi - \theta$ instead of θ, since they are the same up to a change in the viewpoint. In this context, the cell does not own a real orientation with a head and a tail [68], but rather a direction along which it reorients its stress fibers and focal adhesions as a consequence of mechanical stretch. Such a fact is translated in the energy symmetries, leading to configurations which are energetically equivalent. It is clear that, among the invariants appearing in the energy, the one which can lead to symmetry issues is I_8, because it gives rise to terms like $\sin\theta\cos\theta$ which do not preserve the above symmetries. Hence, it is reasonable to assume that U_q depends on I_8 only through its square, leading to $K_{\parallel s} = K_{\perp s} = 0$. For the sake of completeness, in Appendix A we also discuss the case $K_{\parallel s}, K_{\perp s} \neq 0$, showing that their introduction provokes a symmetry breaking which is not biologically feasible, unless one needs to account for other directional cues.

Instead, concerning U_ℓ, we firstly drop the dependence on I_8 for the same symmetry reasons discussed above. Moreover, we observe that, in the linearized case, the contribution of $\hat{I}_3$ is equivalent to the one of $\hat{I}_1$. In fact, since $\mathbb{C} \approx \mathbb{I} + 2\mathbb{E}$, we have that

$$\hat{I}_1 = \mathrm{tr}(\mathbb{C}) - 2 \approx 2\,\mathrm{tr}(\mathbb{E}) \approx \hat{I}_3,$$

neglecting terms of higher order. Consequently, the dependence on $\hat{I}_3$ can be dropped and merged with the one on $\hat{I}_1$. Finally, since we are considering a quadratic approximation of the energy in the linear regime, the only admissible couplings between the other invariants are $\hat{I}_1\hat{I}_4$ and $\hat{I}_1\hat{I}_6$, because products involving $\hat{I}_2$ would have a higher order. Therefore, the dependence on $\hat{I}_2$ can be neglected as well, and the most general expression of the coupling term becomes

$$U_\ell\left(\hat{I}_1, \hat{I}_4, \hat{I}_6\right) = 2K_{14}(\mathrm{tr}\,\mathbb{E})(\mathbf{N}\cdot\mathbb{E}\mathbf{N}) + 2K_{16}(\mathrm{tr}\,\mathbb{E})(\mathbf{N}_\perp\cdot\mathbb{E}\mathbf{N}_\perp)\,,$$

or, as a function of θ,

$$U_\ell(\theta) = 2\varepsilon^2(1-r)\Big[(K_{14} - K_{16})\xi(\theta) + (K_{16} - rK_{14})\Big],$$

where K_{14} and K_{16} are coefficients that weigh the coupling between the three invariants involved.

Since we want to study in more detail the equilibrium orientations and their stability, we take the first derivative of the overall energy with respect to θ and obtain

$$
\begin{aligned}
U'(\theta) &= U_q'(\theta) + U_\ell'(\theta) \\[2mm]
&= \varepsilon^2\Big\{ K_\parallel\left[\xi(\theta) - r\right] + K_\perp\left[\xi(\theta) - 1\right] + \left(\frac{1}{2}K_s + K_{\parallel\perp}\right)\left[r + 1 - 2\xi(\theta)\right]
\end{aligned}
$$

11

$$+2(K_{14} - K_{16})(1 - r)\Big\}\xi'(\theta)\,. \tag{23}$$

Before going on, we notice that such a derivative vanishes for $\theta = \pi/4$ when $r = 1$, since in this case $\xi(\pi/4) = 1$. This fact is coherent with experimental observations [40] suggesting that $\pi/4$ is an equilibrium orientation when the biaxiality ratio amounts to 1, i.e., $\lambda_x = 1 + \epsilon$ and $\lambda_y = 1 - \epsilon$.

In order to rewrite the expression (23) in a more compact form, we define

$$\widehat{K}_{\parallel} := K_{\parallel} + 4K_{14}\,, \qquad \widehat{K}_{\perp} := K_{\perp} + 4K_{16}\,, \qquad K_m := \frac{1}{2}K_s + K_{\parallel\perp} + 2K_{14} + 2K_{16}\,, \tag{24}$$

so that

$$U'(\theta) = \varepsilon^2 \Big\{ \widehat{K}_{\parallel}\left[\xi(\theta) - r\right] + \widehat{K}_{\perp}\left[\xi(\theta) - 1\right] + K_m\left[1 + r - 2\xi(\theta)\right]\Big\}\xi'(\theta)$$

$$= \varepsilon^2 \Big[A\xi(\theta) - B(r + 1) + C\Big]\xi'(\theta)\,, \tag{25}$$

setting

$$A := \widehat{K}_{\parallel} + \widehat{K}_{\perp} - 2K_m\,, \qquad B := \widehat{K}_{\parallel} - K_m\,, \qquad C := \widehat{K}_{\parallel} - \widehat{K}_{\perp}\,. \tag{26}$$

Since, under mechanical stretch, cell stress fibers are mainly aligned to the preferred direction, coherently with [6] in the following we will take $\widehat{K}_{\parallel} > \widehat{K}_{\perp}$. As a consequence, C is always positive, while the sign of A and B cannot be determined a priori, since it depends on the relative magnitude of the various coefficients involved.

Finally, to study the stability of the equilibrium orientations we will need to examine the sign of the second derivative of the energy, which reads

$$U''(\theta) = \varepsilon^2 \Big\{ A\xi'(\theta)^2 + [A\xi(\theta) - B(r + 1) + C]\,\xi''(\theta)\Big\}\,. \tag{27}$$

3.2 Equilibrium Orientations and Stability

Recalling (25), the equilibrium orientations are given by

$$\theta \,:\, \xi'(\theta) = 0 \;\text{ i.e. }\; \theta = k\pi/2,\, k \in \mathbb{Z} \qquad \text{or} \qquad \theta \,:\, A\xi(\theta) - B(r + 1) + C = 0\,,$$

the latter meaning

$$\cos^2\theta = \frac{B}{A} - \frac{C}{A}\frac{1}{1 + r} = \frac{1}{2} + \mathcal{K}\left(\frac{1}{2} - \frac{1}{1 + r}\right)\,, \tag{28}$$

where we have defined

$$\mathcal{K} := \frac{C}{A} = \frac{\widehat{K}_{\parallel} - \widehat{K}_{\perp}}{\widehat{K}_{\parallel} + \widehat{K}_{\perp} - 2K_m}\,. \tag{29}$$

So, in addition to the angles $\theta = k\frac{\pi}{2}$, one might have other four symmetric equilibrium angles given by (28) that depend only on the combination of parameters contained in $\mathcal{K}$. For simplicity, we will denote these configurations as *oblique* equilibria, while those with $\theta = k\pi$ will be referred to as *parallel* equilibria and those with $\theta = \frac{2k+1}{2}\pi$ as *perpendicular* equilibria, where the definition of parallel and perpendicular obviously refers to the stretching direction.

As we shall see, the discussion will depend on the sign of $\mathcal{K}$ (i.e., whether A is positive or negative, having observed that $C > 0$) and whether $|\mathcal{K}|$ is smaller or larger than 1. For this

12

purpose it is useful to define

$$\rho_{\parallel} := \frac{\mathcal{K} - 1}{2\mathcal{K}} = \frac{K_m - \widehat{K}_{\perp}}{\widehat{K}_{\parallel} - \widehat{K}_{\perp}},$$

$$\rho_{\perp} := \frac{\mathcal{K} + 1}{2\mathcal{K}} = \frac{\widehat{K}_{\parallel} - K_m}{\widehat{K}_{\parallel} - \widehat{K}_{\perp}}, \tag{30}$$

$$\rho := \frac{\mathcal{K} + 1}{\mathcal{K} - 1} = \frac{\widehat{K}_{\parallel} - K_m}{K_m - \widehat{K}_{\perp}}.$$

Then, the existence of the oblique equilibrium angle depends on the value of the biaxiality ratio r. Namely, referring to Fig. 2, the equilibrium orientation defined by (28) exists if

$$\rho_{\parallel} < \frac{1}{1 + r} < \rho_{\perp} \quad \text{or} \quad \frac{1}{\rho} < r < \rho \quad \text{when} \quad \mathcal{K} > 1,$$

$$0 < \frac{1}{1 + r} < \rho_{\perp} \quad \text{or} \quad r > \frac{1}{\rho} \quad \quad \text{when} \quad 0 < \mathcal{K} < 1,$$

$$0 < \frac{1}{1 + r} < \rho_{\parallel} \quad \text{or} \quad r > \rho \quad \quad \text{when} \quad -1 < \mathcal{K} < 0,$$

$$\rho_{\perp} < \frac{1}{1 + r} < \rho_{\parallel} \quad \text{or} \quad \rho < r < \frac{1}{\rho} \quad \text{when} \quad \mathcal{K} < -1.$$

Looking at the stability of this orientation, recalling (27) one readily has that the second derivative evaluated in this configuration is $U''(\theta) = \varepsilon^2 A \xi'(\theta)^2$, which is positive provided that $A > 0$. So, if the coefficient A is positive, or equivalently if $\mathcal{K} > 0$, the oblique equilibrium angle turns out to be stable. Otherwise, if the combination of elastic coefficients in A becomes negative, the oblique orientation is unstable.

Looking instead at parallel orientations, e.g., $\theta = 0$, we have that

$$U''(0) = -2\varepsilon^2(r + 1)[(A - B)(r + 1) + C]. \tag{31}$$

Therefore, referring again to Fig. 2 and observing that $A - B = -\rho_{\parallel} C$, such an orientation is stable if

$$\frac{1}{1 + r} < \rho_{\parallel}. \tag{32}$$

Consequently, if $\rho_{\parallel} > 0$ (i.e. if $\mathcal{K} < 0$ or $\mathcal{K} > 1$) the parallel orientation is stable under the condition (32), while if $\rho_{\parallel} < 0$ (i.e. if $0 < \mathcal{K} < 1$) it is always unstable.

Finally, the perpendicular orientations, e.g. $\theta = \pi/2$, are stable if

$$U''\left(\frac{\pi}{2}\right) = -2\varepsilon^2(r + 1)[B(r + 1) - C] > 0, \tag{33}$$

leading to the condition

$$\frac{1}{1 + r} > \rho_{\perp}, \tag{34}$$

or equivalently $r < 1/\rho$. However, if $\mathcal{K} \in (-1, 0)$ the r.h.s. of (34) is negative. So, in this range the perpendicular orientation is always stable, while outside the aforementioned interval stability is granted whenever r satisfies (34).

Taken together, these results show that, as shown in Figs. 2(b), 2(d) for any quadratic orthotropic elastic energy in a linear regime, oblique equilibrium angles follow a straight line in
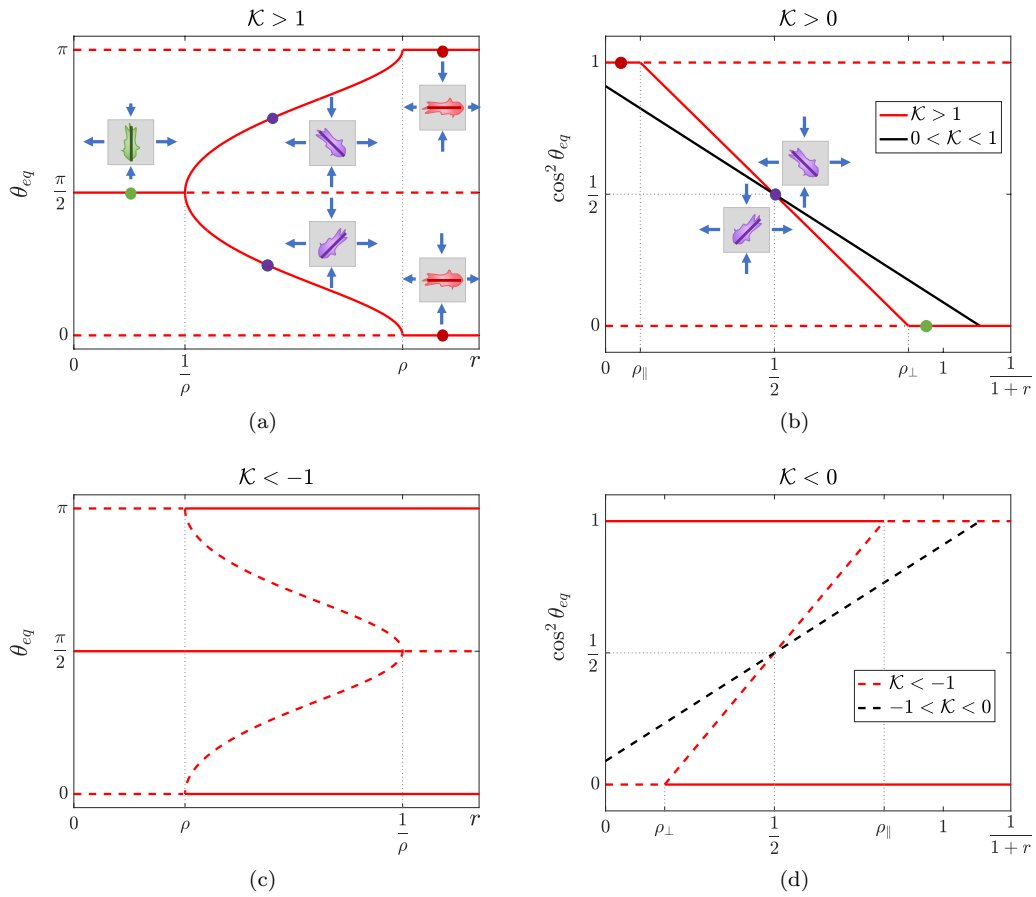
13

Figure 2: Bifurcation diagrams for positive $\mathcal{K}$ (top) and negative $\mathcal{K}$ (bottom). The bifurcation values are obtained for $(1+r)^{-1} = \rho_{\parallel} = (K_m - \widehat{K}_{\perp})/(\widehat{K}_{\parallel} - \widehat{K}_{\perp})$ and $(1+r)^{-1} = \rho_{\perp} = (\widehat{K}_{\parallel} - K_m)/(\widehat{K}_{\parallel} - \widehat{K}_{\perp})$. The insets and dots in (a) and (b) show representative cellular orientations: perpendicular (green), oblique (purple) and parallel (red).

14

the $\left((1+r)^{-1}, \cos^2\theta\right)$ plane upon changes in the values of the biaxiality ratio. This is confirmed by experimental assays: in the set-up of the experiments by Livne et al. [40], collected data of the oblique orientation seem to align along a straight line with $\mathcal{K} = 1.26 \pm 0.08$.

Figure 2 summarizes the above discussion : in Fig. 2(a) and 2(c) we show the bifurcation diagram in the (r, θ) plane for $\mathcal{K} > 1$ and $\mathcal{K} < -1$ respectively, while in Fig. 2(b) and 2(d) we report the straight lines in the $\left((1+r)^{-1}, \cos^2\theta\right)$ plane, for $\mathcal{K} > 0$ and $\mathcal{K} < 0$ respectively. It can be observed that if $\mathcal{K} > 1$ there are two supercritical pitchfork bifurcation points for $r = 1/\rho$ and $r = \rho$. So, for any r there is only one stable equilibrium angle in the interval $\left[0, \frac{\pi}{2}\right]$, and its symmetric counterpart with respect to $\pi/2$ if $r \in \left(\rho^{-1}, \rho\right)$. Hence, changing r one can smoothly pass from a configuration with the cell axis aligned along the stretching direction to one perpendicular to the stretching direction. We observe however that the range of values tested in the experiments is $(1+r)^{-1} \in \left[\frac{1}{2}, 1\right]$, because the substrate is not compressed along y more than it is stretched along x, which would correspond to values of $r > 1$. At the same time, it is not extended simultaneously along x and y, which would lead to negative values of r. This is the reason why, if $0 < \mathcal{K} < 1$, only the oblique equilibrium orientation is stable, while the parallel and perpendicular ones turn out to be always unstable in the experimental range of variation of r. We observe that, since for instance in Livne's experiments they find $\mathcal{K} \approx 1.26$ [40], a constraint can be inferred among the three coefficients appearing in (29), or equivalently among the six parameters in (24). In particular, the fact that $\mathcal{K} > 1$ assures that K_m cannot be neglected, because otherwise $\mathcal{K}$ in (29) would always be smaller than 1. Starting from this observation and recalling that $\widehat{K}_\parallel > \widehat{K}_\perp$, looking for the minimum number of coefficients necessary to satisfy the experimental values, one finds that, on the other hand, $\widehat{K}_\perp$ could be neglected, so that $\mathcal{K}$ can be rewritten in terms of the ratio $K_m/\widehat{K}_\parallel$ as

$$\frac{1}{\mathcal{K}} \approx 1 - 2\frac{K_m}{\widehat{K}_\parallel}.$$

Actually, on the basis of the experimental slope, we can argue that, if $\widehat{K}_\perp = 0$ (i.e. $K_\perp = K_{16} = 0$), then

$$\frac{K_m}{\widehat{K}_\parallel} = \frac{\frac{1}{2}K_s + K_{\parallel\perp} + 2K_{14}}{K_\parallel + 4K_{14}} \approx 0.103\,,$$

that entails $\widehat{K}_\parallel >> K_m$, i.e., the coefficient related to the stiffness to stretching in the direction of cell orientation is higher than all the other parameters. We highlight again that, even though the contribution of K_m is smaller than the one of $\widehat{K}_\parallel$, the former parameter is fundamental to obtain a biologically relevant response.

Looking now at the case $\mathcal{K} < -1$, as in Fig. 2(c), which might for instance occur if K_m is large with respect to $\widehat{K}_\parallel$ and $\widehat{K}_\perp$, then the pitchfork bifurcations become subcritical and one jumps from the parallel to the perpendicular equilibria, since the oblique one is always unstable. So, imagining to operate on K_m, when $2K_m$ passes from being smaller to being larger than $\widehat{K}_\parallel + \widehat{K}_\perp$, corresponding respectively to $\rho_\parallel < \rho_\perp$ and $\rho_\parallel > \rho_\perp$, there is a switch from supercritical to subcritical bifurcations. In Fig. 2(d) we also plot the case $-1 < \mathcal{K} < 0$, in which one has the same bistable behaviour for all the experimental values of r, while the oblique orientation loses its stability. This could be an explanation of why the oblique orientation might not be observed in the case $\mathcal{K} < 0$, that is $\widehat{K}_\parallel + \widehat{K}_\perp < 2K_m$. Differently from previous models, our bifurcation analysis includes this possibility, which however needs to be validated precisely through experimental data.

Moreover, even though experiments are commonly performed in a range of biaxiality ratio $r \in [0, 1]$, our model is able to foresee the behaviour of the cell even for values of $r > 1$, i.e.

$_1$ when the substrate is more compressed in the y-direction than it is stretched in the x-direction,
$_2$ a condition not tested yet experimentally.

$_3$ We finally observe that the presence of pitchfork bifurcations is not surprising, since they
$_4$ often arise in one-dimensional dynamical systems that present some symmetries: this is indeed
$_5$ our case, since we took an energy functional which is even and symmetric with respect to $\pi/2$ in
$_6$ order to match some biological considerations. As a matter of fact, the introduction of $K_{\|s}$ and
$_7$ $K_{\perp s}$, discussed in Appendix A, leads to a symmetry breaking and therefore to the appearance
$_8$ of turning points.

$_9$ # 4 Simulations of the Viscoelastic Model

$_{10}$ After having discussed the equilibrium orientations in Section 3, here we focus on the dynamics
$_{11}$ of cell reorientation in response to the viscoelastic model presented in Section 2, performing some
$_{12}$ numerical simulations. More specifically, we consider the system of equations which describes
$_{13}$ the time evolution of the Cauchy stress tensor $\mathbb{T}$ and the reorientation dynamics of the angle
$_{14}$ θ. As regards the former, its evolution is governed by the viscoelastic constitutive equation (6)
$_{15}$ described in Section 2; concerning the angle, as in Eq. (2) we assume that changes in orientation
$_{16}$ are driven by a dissipative process in which the cell tries to find the direction which minimizes
$_{17}$ the virtual work done by the Cauchy stress. Consequently, the system of equations is

$$\begin{cases} \dot{\theta} = -\dfrac{1}{\widehat{K}_{\|}\lambda_\theta}\dfrac{\partial \mathbb{T}}{\partial \theta} : \mathbb{E}\,, & \text{(35a)} \\[4mm] \dot{\mathbb{T}} + \dfrac{1}{\lambda}\mathbb{T} = \dfrac{1}{\lambda}\mathbb{C}_0\dot{\mathbb{E}}\,, & \text{(35b)} \end{cases}$$

$_{18}$ where $\mathbb{C}_0$ is the functional that accounts for the exponentially weighted history of past orientations
$_{19}$ defined in (7), depending on the elasticity tensor $\mathbb{C}_0$. The components of $\mathbb{C}_0$ can be written in
$_{20}$ terms of θ as

$$(\mathbb{C}_0)_{xxxx} = \widehat{K}_{\|}\cos^4\theta + \widehat{K}_{\perp}\sin^4\theta + 2K_m\sin^2\theta\cos^2\theta\,,$$

$$(\mathbb{C}_0)_{yyyy} = \widehat{K}_{\|}\sin^4\theta + \widehat{K}_{\perp}\cos^4\theta + 2K_m\sin^2\theta\cos^2\theta\,,$$

$$(\mathbb{C}_0)_{xxyy} = K_m - \frac{1}{2}K_s + (\widehat{K}_{\|} + \widehat{K}_{\perp} - 2K_m)\sin^2\theta\cos^2\theta\,.$$

$_{21}$ We consider a specimen stretched in the x-direction uniformly with a fixed biaxiality ratio r,
$_{22}$ such that the infinitesimal deformation tensor is given by (20) with

$$\varepsilon(t) = \frac{1}{2}\varepsilon_0(1 - \cos\omega t)\,,$$

$_{23}$ for different angular frequencies. Compared to experiments, in the simulations we do not assume
$_{24}$ that the oscillation period is smaller or greater than the characteristic relaxation time λ or
$_{25}$ reorientation time λ_θ, in order to put in evidence both the elastic and the viscous behaviour of
$_{26}$ the system.

       We now solve Eq. (35) for a range of values of r to check the theoretical predictions obtained
through the bifurcation analysis. In particular, a numerical algorithm has been implemented
using MATLAB$^{\circledR}$. As regards Eq. (35b), its discretization was performed through the explicit
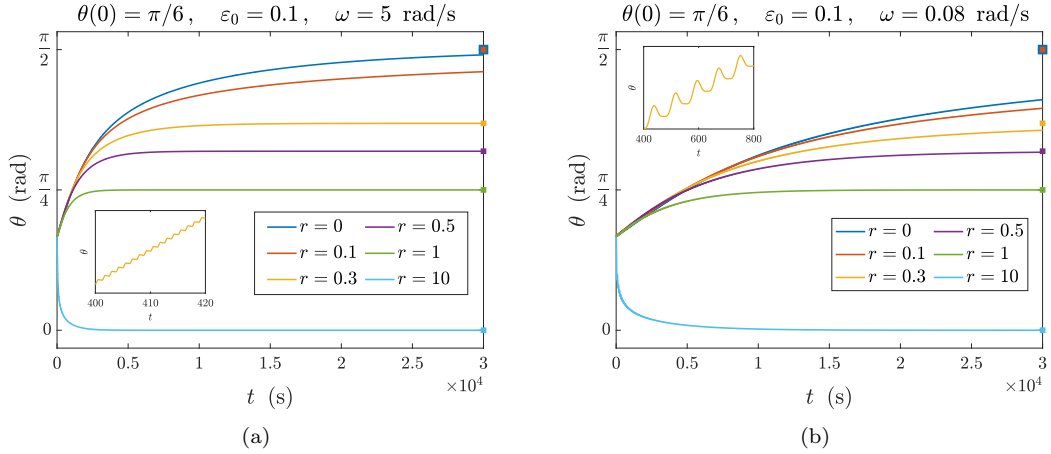
Figure 3: Evolution of θ according to (35) in the high frequency (a) and low frequency (b) cases, for $\mathcal{K} = 1.26$ and $\varepsilon_0 = 0.1$, while the biaxiality ratio r is varied. As initial condition, we take in both cases $\theta(0) = \pi/6$. The squares on the right of each plot highlight the steady orientations predicted by the bifurcation analysis. Moreover, all curves display an oscillatory behaviour, as shown in the insets for the specific case $r = 0.3$.

Euler method. It is equivalent to two scalar equations for the components T_{xx}, T_{yy} of the Cauchy tensor $\mathbb{T}$: the integrals in the r.h.s. of (35b) have been approximated observing that, for instance in the case $r = 0$,

$$(\mathbb{C}_0^{k+1})_{xxxx} = \int_{-\infty}^{t_{k+1}} e^{-(t_{k+1}-\tau)/\lambda} \, (\mathbb{C}_0)_{xxxx}(\theta(\tau)) \, d\tau$$

$$= e^{-(t_{k+1}-t_k)/\lambda} (\mathbb{C}_0^k)_{xxxx} + \int_{t_k}^{t_{k+1}} e^{-(t_{k+1}-\tau)/\lambda} \, (\mathbb{C}_0)_{xxxx}(\theta(\tau)) \, d\tau. \tag{36}$$

1. Then, with an analogous procedure, all the integral terms can be evaluated from the value
2. at the previous time instant plus the discretization of the remaining integral in (36), which
3. was performed through the trapezoidal rule. The generalization to the case $r \neq 0$ is then
4. straightforward. Finally, concerning the virtual work term in Eq. (35a), the derivative of the
5. stress with respect to θ was approximated using a centered finite difference. In all our simulations
6. we take $\lambda = \lambda_\theta = 6.6\,\mathrm{s}$ and to have coherence with experimental data we consider a value of
7. $\mathcal{K} = 1.26$ [40]. Instead, we focus on the effect of variations of r, ε_0 and ω to evaluate their impact
8. on the reorientation dynamics of the cell.
9. In Figure 3(a) we show the evolution of the orientation angle in the high frequency case,
10. starting from an initial condition $\theta(0) = \pi/6$, for different values of r. We see that the angle
11. approaches the value obtained in Section 3.2 in the stationary case (identified by a coloured
12. marker on the the right side of the box) and reported in the bifurcation diagrams in Fig. 2.
13. More specifically, for low values of r the final orientation is almost orthogonal to the direction
14. of stretching. Increasing the biaxiality ratio r makes the equilibrium angle decrease, reaching
15. the expected value given by the bifurcation diagrams: in particular, we observe that the steady
16. angle is $\pi/4$ when $r = 1$, as predicted by the theory and by the experiments. For the sake of
17. completeness, we also showed a case in which $r \gg 1$, even if no experimental data are available

17

in this case: in this situation one has $\theta \to 0$, coherently with the study carried out in Section 3. We also studied the behaviour of the angle reorientation for a different initial condition greater than $\pi/2$, that is $\theta(0) = 5\pi/6$ (not shown in the Figures): as before, the evolution towards the steady angle is predicted by the bifurcation diagram for all values of r. In fact, such a choice for the initial condition makes the system go to the other mirror-image orientation, greater than $\pi/2$ and finally, for large values of r, to $\theta = \pi$. We recall however that the last configuration is biologically equivalent to $\theta = 0$ because of the discussed symmetries of the energy, implying that the cell is aligned with the x-axis.

Conversely, in Figure 3(b), we report the plots of θ in the low frequency regime for the same initial condition, choosing $\omega = 0.08$ rad/s which is slightly above the experimental reorientation threshold of 0.06 rad/s suggested for experiments. The dynamics is coherent with model predictions: we have the same equilibria as in the high frequency case, even if the convergence towards the steady angle is slower due to the presence of viscous effects. As shown in the inset plots in Fig. 3(a) and Fig. 3(b), all curves display an oscillatory behaviour as expected, since we are imposing a periodic deformation to the specimen. Hence, the orientation angle progressively increases through small oscillations until it reaches the predicted orientation. In particular, such oscillations are smaller in amplitude and faster in the elastic case, while they have a greater amplitude and are slower in the viscous limit.

To compare our results with reorientation frequencies and thresholds from Jungbauer et al. [30], we performed some simulations for their same experimental biaxiality ratio and amplitude, changing instead the value of ω. As shown in Fig. 4(a), angular frequencies below a minimum threshold (which can be quantified in about 0.01 Hz ≈ 0.06 rad/s, which is coherent with experiments on some cell types [28, 30]) do not induce a significant or significantly fast response. In this case, the reorientation is so slow that it cannot be seen on time scales comparable with the cell cycle, and in the experimental case the process is destroyed by random fluctuations. Instead, higher frequencies induce reorientation, with a characteristic time that, coherently with [30], decreases with the frequency. This is true until ω reaches a second threshold of about 2π rad/s (i.e. 1 Hz), after which a further increase in the frequency does not substantially accelerate the reorientation process towards the expected equilibrium angle. This is confirmed and summarized by the results in Fig. 4(b), where we report the average speed of reorientation v_m, calculated over a suitable interval where each curve can be approximated by a line, as a function of the frequency of the imposed deformation. We find that the speed of reorientation is very low when $\omega < 0.01$ rad/s, corresponding to evolution times of the order of days. Then, there is a sudden transition interval for $\omega \in [0.01, 1]$ rad/s with an inflection point close to $\omega \approx 0.15$ rad/s, i.e. when $\lambda\omega \approx 1$, related to the viscous-elastic transition in the material. Finally, for higher values of ω, the speed of reorientation saturates to values corresponding to experimental times of the order of an hour. To make a further comparison with experiments, we define the characteristic time of reorientation for our model as $\tau := (\theta_{eq} - \theta_0)/v_m$, assuming that the evolution curves for θ as a function of time are approximated by a saturating exponential. Then, in Fig. 4(c) we plot this characteristic time together with data for rat embryonic fibroblasts (REF cells) from [30]. As discussed before, such a time decreases with the frequency until a threshold, above which it remains almost constant, and the model predictions show a good agreement with experimental data.

In Figure 5 we studied instead the influence of the stretch amplitude ε_0, while the angular frequency is kept high in Fig. 5(a) and low in Fig. 5(b), fixing $r = 1$ and therefore $\theta_{eq} = \pi/4$. As one could expect, the equilibrium orientation for a given initial condition $\theta(0)$ and biaxiality ratio r is not altered by variations of ε_0 and remains equal to $\pi/4$ in this case. Changes in the amplitude only influence the speed of convergence towards the predicted equilibrium angle. Indeed, if we scale times with $1/\omega$, the stress tensor with $\widehat{K}_\parallel \varepsilon_0$, and the strain tensor with ε_0,
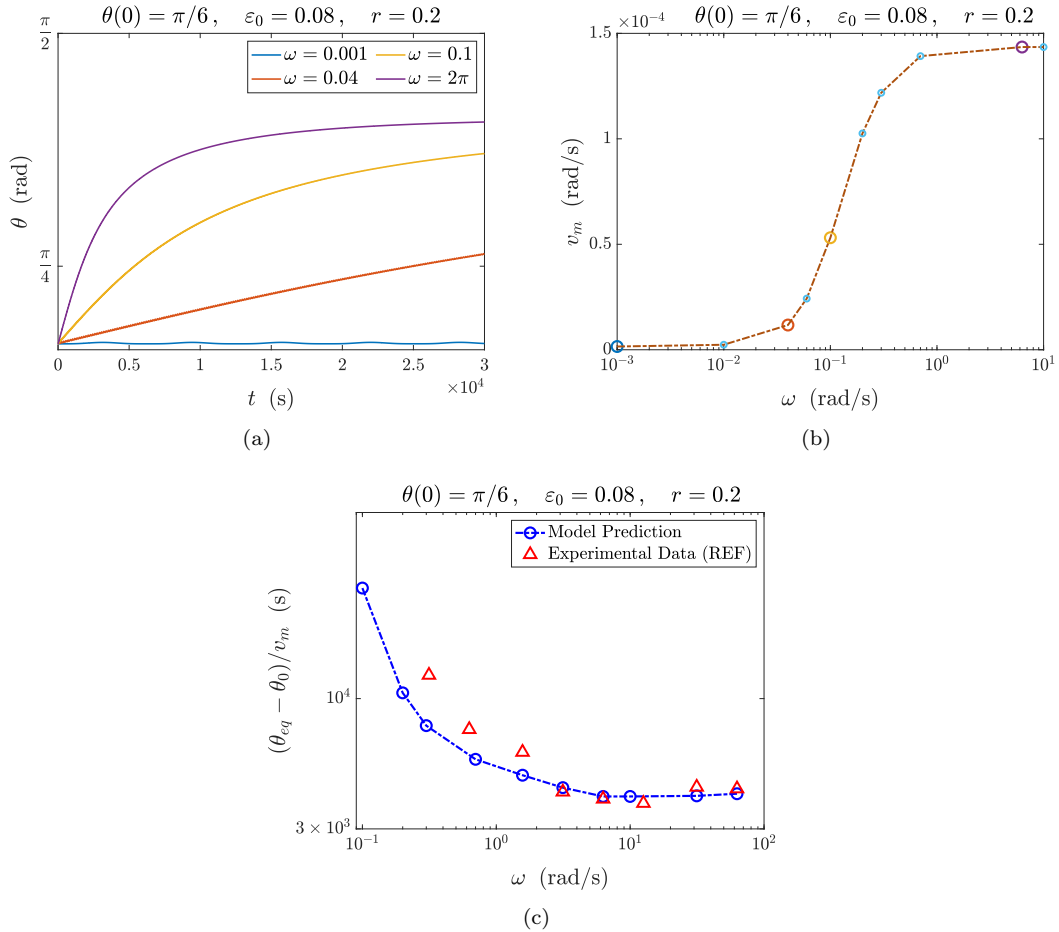
18

Figure 4: (a): Evolution of θ according to (35) for a fixed biaxiality ratio and different angular frequencies. We observe that low frequencies (approximately below a minimum threshold of 0.06 rad/s, i.e., about 0.01 Hz, coherently with experimental results [28, 30]) do not induce a significant reorientation response. For higher frequencies, the preferential orientation becomes visible and the reorientation time decreases. (b): Average speed of reorientation v_m, computed in a suitable interval where the evolution curve is approximately linear, as a function of the imposed angular frequency in logarithmic scale. Recalling that we used $\lambda = \lambda_\theta = 6.6\,\text{s}$, a transition occurs when $\lambda\omega = 1$, i.e., the inflection point in $\omega \approx 0.15$ rad/s. Then, there is a second threshold of about 2π rad/s, above which a further increase does not induce a significantly faster response [30]. (c): Plot of the model characteristic time $\tau := (\theta_{eq} - \theta_0)/v_m$ as a function of the angular frequency in logarithmic scale, together with experimental results for rat embryonic fibroblasts (REF cells) taken from [30].
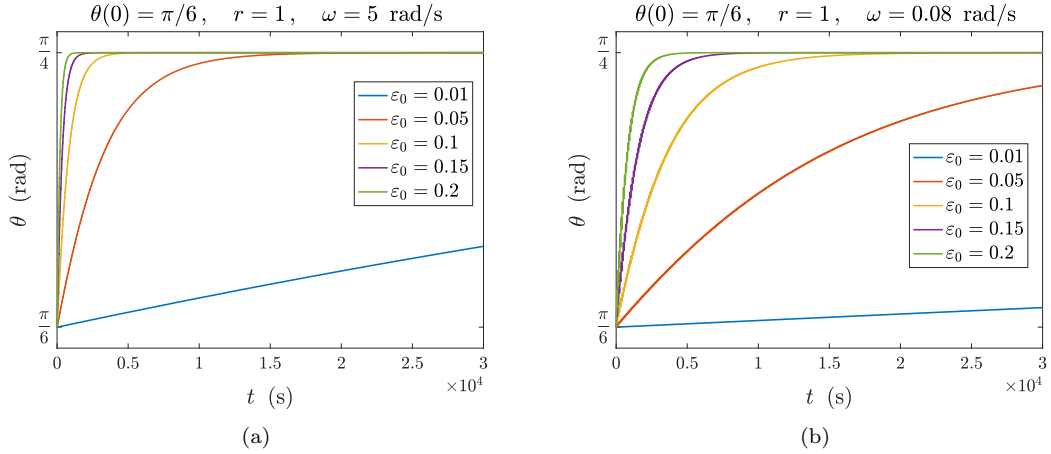
Figure 5: Evolution of θ according to (35) in (a) the high frequency and (b) the low frequency cases for different values of the stretch amplitude ε_0 and fixed biaxiality ratio $r = 1$.

the system (35) rewrites in dimensionless terms formally substituting $\widehat{K}_\parallel \lambda_\theta$ with $\widetilde{\Lambda}_\theta = \lambda_\theta \omega / \varepsilon_0^2$ and λ with $\widetilde{\Lambda} = \lambda \omega$. In formulas, defining $t = \widetilde{t}/\omega$, $\mathbb{T} = \widetilde{\mathbb{T}} \widehat{K}_\parallel \varepsilon_0$, $\mathbb{E} = \widetilde{\mathbb{E}} \varepsilon_0$ and $\mathbb{\mathcal{C}}_0 = \widetilde{\mathbb{\mathcal{C}}}_0 \widehat{K}_\parallel \lambda$ yields

$$
\begin{cases}
\dfrac{d\theta}{d\widetilde{t}} = -\dfrac{1}{\widetilde{\Lambda}_\theta} \dfrac{\partial \widetilde{\mathbb{T}}}{\partial \theta} : \widetilde{\mathbb{E}} \,, & \text{(37a)} \\[2ex]
\dfrac{d\widetilde{\mathbb{T}}}{d\widetilde{t}} + \dfrac{1}{\widetilde{\Lambda}} \widetilde{\mathbb{T}} = \widetilde{\mathbb{\mathcal{C}}}_0 \dfrac{d\widetilde{\mathbb{E}}}{d\widetilde{t}} \,. & \text{(37b)}
\end{cases}
$$

As already discussed in Sections 2.1 and 2.2, the former dimensionless group $\widetilde{\Lambda}_\theta$ is related to the time needed by the cell to re-orientate in terms of the oscillation frequency and amplitude, while the latter $\widetilde{\Lambda}$ identifies the relative role of viscoelasticity. In particular, focusing on $\widetilde{\Lambda}_\theta$, if the amplitude of oscillation increases (e.g., doubles) the evolution of the orientation angle θ remains the same provided that the reorganization time λ_θ is suitably increased (e.g., quadruples). On the other hand, if λ_θ is kept constant, as done in Fig. 5, cells re-orient faster, and the re-orientation time scales like the square of the oscillation amplitude. However, to simplify the direct comparison with experimental results, we decided to perform all simulations using dimensional quantities.

Finally, in Figure 6 we report the evolution of the Cauchy stress components T_{xx} and T_{yy}, both normalized with respect to $\widetilde{K}_\parallel$. In particular, Figs. 6(a) and 6(b) show the stresses in the high frequency case, for a fixed biaxiality ratio $r = 0.3$. It can be observed that, starting from a stress-free configuration, there is a first increase in both stress values up to a peak, after which relaxation begins and completes in about 100 seconds. Once the transient is passed, the stress components start to oscillate around zero, meaning that the system is behaving purely elastically. In the low frequency case, plotted in Fig. 6(c) and 6(d), the response of the system is much slower, since the viscous component emerges visibly. Concerning the stress magnitude when the equilibrium orientation is reached, as predicted by the model, we observe that the stress components in the low frequency case differ from the ones in the high frequency case by a factor $\lambda \omega_{low} \approx 0.53$.

20

We have to stress that, in all simulations, we kept the characteristic times λ and λ_θ constant, to better identify the effects of the oscillation characteristics in terms of frequency and amplitude. However, the dynamics of adhesion to the substrate is more involved because the application of a stress on them has the consequence of both strengthening the bonds, due to an increased clustering of integrins, and prolonging their lifetime. In particular, two types of bonds are identified in the literature, catch and slip bonds [34, 37, 72, 75, 76]. Increasing the applied deformation has the effect of increasing the applied force acting on the bonds and this causes a decrease (resp., an increase) of the lifetime of slip (resp., catch) bonds. So, the dependence of the adhesion bond lifetime, and therefore of λ, on the deformation is not constant and might actually not even be monotone with a maximum corresponding to an applied force of the order of $10\,\mathrm{pN}$. However, as discussed in Sections 2.1 and 2.2, including such a strain-dependence lifetime would not change the equilibrium configuration, but only the temporal behaviour of the system. Conversely, a strengthening of the adhesion bond might change both, though we do not expect them to be relevant.

5 Discussion

The response of cells to mechanical cues is a relevant biological phenomenon which still needs investigations and efforts to be enlightened. Starting from experimental observations showing that, when a monolayer is subject to a biaxial stretch, cells orient themselves in a well-defined configuration, in this paper we employed mechanical instruments to further explore this behaviour, focusing on linear elasticity and viscoelasticity. Previous works [40, 42] suggested that a linear elastic model is able to fit the experimental data for a wide range of strain energies, while the impact of nonlinearities seems slight.

To account for viscous effects during the reorientation process, due for instance to formation and breaking of integrin bonds between the cell and the substrate, we developed a viscoelastic model which describes the system as an anisotropic continuum with preferential directions induced by the presence of stress fibers and lateral protein network. This allowed us to differentiate the behaviour depending on the period of the applied cyclic stretch: if the latter is much shorter than the cell characteristic response times λ and λ_θ, then the response is elastic with cells having not enough time to reorganize. On the other hand, if the imposed frequency is low, viscous-like behaviours emerge slowing down the reorientation, until the process becomes too slow to be relevant. We showed that our viscoelastic model is able to capture these differences, which can be recovered by taking the limit of the general constitutive equation in the high and low frequency cases.

Then, we studied in detail the steady orientations with two main objectives: to generalize previous linear elastic models using the most general orthotropic model and to analyze the bifurcations that occur when the biaxiality ratio of the deformation is changed. In particular, we considered a general quadratic strain energy involving a priori six elastic parameters: $\widehat{K}_\parallel$ and $\widehat{K}_\perp$, related to the stiffness along the cell major axis and along the orthogonal direction, respectively; K_s, modelling the resistance to shear; and $K_{\parallel\perp}$, $K_{\parallel s}$, $K_{\perp s}$ including coupled effects among the previous three. The bifurcation analysis is coherent with previous theoretical and experimental works [23, 40, 42], and a linear relation between the parameter $\frac{1}{1+r}$ and $\cos^2\theta$, where θ is the nontrivial equilibrium orientation, is recovered. The slope of the line is given by the combination of elastic coefficients

$$\mathcal{K} = \frac{\widehat{K}_\parallel - \widehat{K}_\perp}{\widehat{K}_\parallel + \widehat{K}_\perp - 2K_m},$$
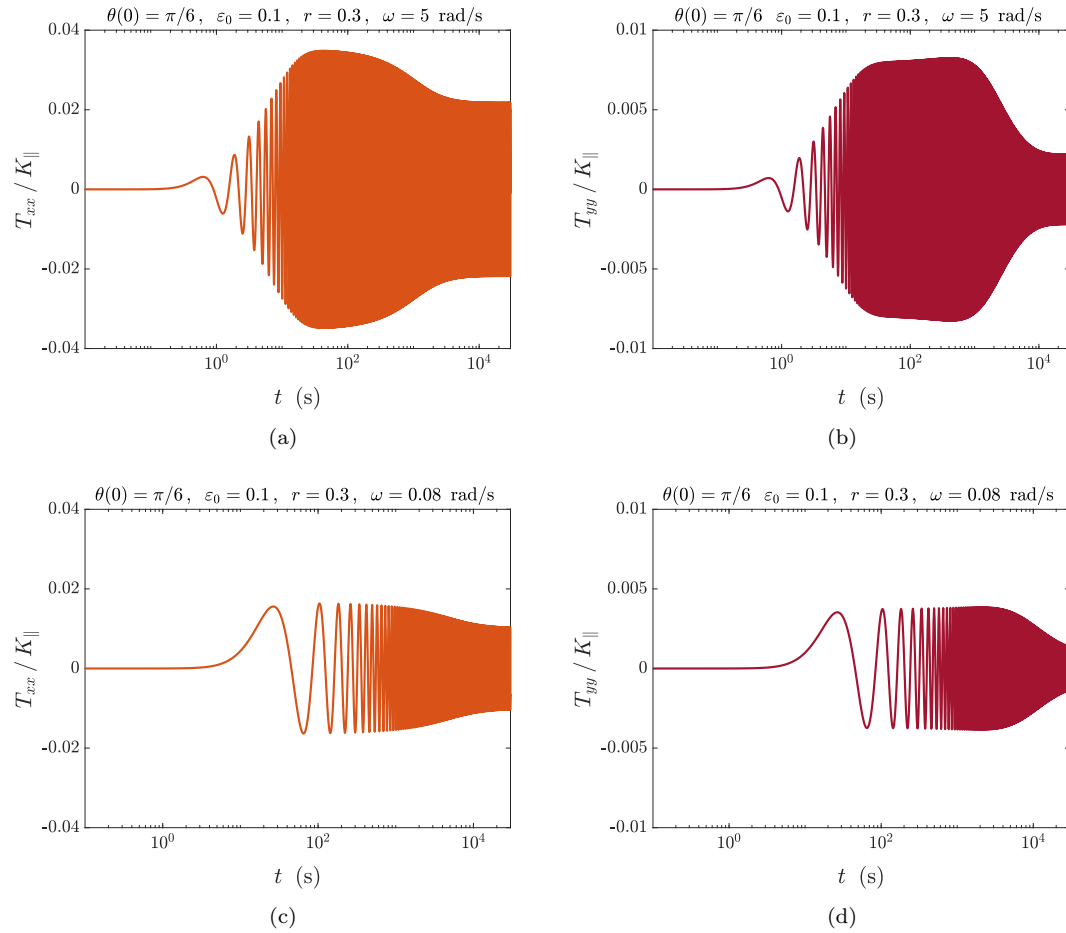
21

Figure 6: Time evolution of the stress tensor components T_{xx} and T_{yy} (normalized w.r.t. $\widetilde{K}_{\parallel}$), for $r = 0.3$. In the top row the high frequency case is reported, while in the bottom row the plots refer to the low frequency case. The time axis is reported in logarithmic scale to put in evidence the temporal behaviour of stress amplitudes.

which in some experimental results was reported to be about 1.26 ± 0.08 [40]. The value of the experimental slope allowed to conclude that the presence of a non negligible response to shear given by K_m is important as well as the major role played by the response to stretch along the direction of cell orientation (given by $K_\parallel$).

Our description also allows a continuous variation of $\mathcal{K}$, which can achieve positive or negative values depending on the parameters appearing in its definition: even if, to our knowledge, there are no experimental data available for situations like $\mathcal{K} < 0$, our elastic model is in principle able to capture them. Moreover, differently from our previous work [42], we included in the energy possible isotropic-anisotropic couplings: as we have seen, their introduction does not qualitatively alter the results and the linear relation between $1/(1+r)$ and $\cos^2 \theta$, but only leads to a redefinition of some parameters.

In detail, we observed two supercritical pitchfork bifurcations when $\mathcal{K} > 1$: for low values of the biaxiality ratio r the orthogonal orientation is stable, while two specular equilibria become stable after the first bifurcation. Increasing r even more they finally disappear, leaving the orientation $\theta = 0$ or $\theta = \pi$ as stable. Instead, if $\mathcal{K} < -1$, the two bifurcations become subcritical. The presence of pitchfork bifurcations is coherent with the energy symmetries. In fact, in our framework the orientations $\theta, -\theta, \pi - \theta, \pi + \theta$ are energetically equivalent, because the cell only chooses a direction without distinction between head and tail.

Simulations in the case $\mathcal{K} > 0$ confirmed the analytical predictions, showing an evolution towards a steady angle depending on the imposed biaxiality ratio and on the initial condition, but not on the frequency. Although experiments are still needed to deeply investigate such a behaviour of the cells, to our knowledge there is some agreement in the literature on the fact that the preferred orientation angle does not directly depend on the frequency of the cyclic deformation. Instead, the frequency seems to influence the amount of cells found oriented along the preferential direction and the speed of the cytoskeletal response [23, 30, 43, 62]. This latter effect is evident in our simulations where we have shown that, in the low frequency case, convergence is slowed down due to the presence of viscous effects, even if the stationary orientation is still predicted by the bifurcation diagrams. Moreover, in accordance with the results in [28, 30], there is a transition for $\lambda\omega \approx 1$, so that the time required to observe reorientation is of the order of days for small ω's, saturating to one hour for larger frequencies.

Hence, our model seems consistent with previous experimental data and theories describing the behaviour of an ensemble of cells on a stretched substrate, also discussing the case of isotropic-anisotropic couplings in the energy and recovering once more the established linear relation between the squared cosine of the angle and a parameter related to the deformation.

However, there are at least three aspects that are not covered yet by the present modelling framework and will be the aim of future works. The first one concerns the influence of the compliance of the substratum, the second one is related to the dependence of the viscoelastic parameters describing the mechanical behaviour of adhesion molecules on the applied deformation or stress, and the third involves the response of cells cultured on monolayer undergoing a static step deformation. This last effect is still debated since some experimental assays showed that, differently from the cyclic case, cells stress fibers or focal adhesions may prefer the parallel orientation [11, 15, 17, 22] also in a pre-stretched condition [39], while other studies reported different results or even no reorientation at all [25, 38]. Further investigation is required in this regard, since experimental conditions are very different from one another. Introducing remodelling of cell cytoskeleton and stress fibers, following an active fiber reorientation approach [12, 13], may be a direction for future research and modelling, on which we are currently focusing.

Moreover, in this work we considered a purely homogeneous deformation since we wanted to make analytical considerations and to carry out a detailed bifurcation analysis. However, to realistically reproduce the experimental settings, it would be more accurate to impose the strain

23

only at the boundary of the specimen: this requires a computational effort to solve the elastic problem, using for instance a finite element scheme. Finally, another possible perspective for future improvement would be to account for the mechano-chemical response of the cell at the microscopic scale, considering for instance active mechanotransduction in a multiscale framework. The inclusion of active effects like shape fluctuations, metabolism [20] and cell response to topographical cues in the substrate, even in absence of external mechanical stimuli [4], could be of help in understanding the complex interactions between the cell and its environment.

A   The Asymmetric Case

In this Appendix, we turn our attention to a more general case for which $K_{\perp s}, K_{\parallel s} \neq 0$ in the anisotropic energy (22), to show that their introduction leads to a symmetry breaking bifurcation. If we do not neglect the contribution of these parameters, the overall strain energy as a function of θ becomes

$$
\begin{aligned}
U(\theta) = \frac{1}{2}\varepsilon^2 \Big\{ & K_{\parallel}[\xi(\theta) - r]^2 + K_{\perp}[1 - \xi(\theta)]^2 + K_s\,\xi(\theta)[r + 1 - \xi(\theta)] \\
& + 2K_{\parallel\perp}[\xi(\theta) - r][1 - \xi(\theta)] - 2K_{\parallel s}[\xi(\theta) - r](r+1)\sin\theta\cos\theta \\
& - 2K_{\perp s}[1 - \xi(\theta)](r+1)\sin\theta\cos\theta \Big\} \\
& + 2\varepsilon^2(1 - r)\Big[(K_{14} - K_{16})\xi(\theta) + (K_{16} - rK_{14}) \Big],
\end{aligned}
\tag{A.1}
$$

while its first derivative is

$$
\begin{aligned}
U'(\theta) = \varepsilon^2 \Big\{ & \Big[K_{\parallel}\left[\xi(\theta) - r\right] + K_{\perp}\left[\xi(\theta) - 1\right] + \left(\frac{1}{2}K_s + K_{\parallel\perp}\right)[r + 1 - 2\xi(\theta)] \\
& - \left(K_{\parallel s} - K_{\perp s}\right)(r+1)\sin\theta\cos\theta + 2(K_{14} - K_{16})(1 - r) \Big]\xi'(\theta) \\
& - \Big[K_{\parallel s}[\xi(\theta) - r] + K_{\perp s}[1 - \xi(\theta)] \Big](r+1)(\cos^2\theta - \sin^2\theta) \Big\}.
\end{aligned}
\tag{A.2}
$$

Before going further, we observe that, in order to have coherence with the experimental condition $U'(\pi/4) = 0$ for $r = 1$ (which was automatically granted in the case $K_{\parallel s} = K_{\perp s} = 0$), the following constraint is necessary:

$$
K_{\parallel s} = K_{\perp s}.
$$

Hence, we have that the mixing contributions related to shear must be equal. Under this condition, the energy derivative rewrites as

$$
U'(\theta) = \varepsilon^2 \Big\{ [A\xi(\theta) - B(r+1) + C]\xi'(\theta) + K_{\parallel s}(r^2 - 1)(\cos^2\theta - \sin^2\theta) \Big\},
\tag{A.3}
$$

where A, B and C are defined as in (26). Then, differently from Eq. (25), we have an additional contribution related to $K_{\parallel s}$.

In this situation, to derive the equilibrium orientations, we try to write them expliciting r instead of $\cos^2\theta$ when imposing that $U'(\theta) = 0$. Therefore, we have that the steady state angles satisfy

$$
2[A(r+1)\cos^2\theta - B(r+1) + C]\sin\theta\cos\theta + (1 - r)K_{\parallel s}(\cos^2\theta - \sin^2\theta) = 0,
$$

that can be readily solved yielding

$$r = \frac{K_{\|s}(\cos^2\theta - \sin^2\theta) + 2(A\cos^2\theta - B + C)\sin\theta\cos\theta}{K_{\|s}(\cos^2\theta - \sin^2\theta) - 2(A\cos^2\theta - B)\sin\theta\cos\theta} \ . \tag{A.4}$$

Actually, as in the symmetric case $K_{\|s} = 0$, a more compact form only depending on a single parameter can be achieved working in terms of $\frac{1}{1+r}$. In fact, with this idea (A.4) rewrites as

$$\frac{1}{1+r} = \frac{C\sin 2\theta - A\sin 2\theta\cos 2\theta + 2K_{\|s}\cos 2\theta}{2(2K_{\|s}\cos 2\theta + C\sin 2\theta)} = \frac{1}{2}\left[1 - \frac{1}{\mathcal{K}}\frac{\sin 2\theta\cos 2\theta}{\sin 2\theta + 2\gamma\cos 2\theta}\right] , \tag{A.5}$$

where $\mathcal{K}$ is defined in (29) and

$$\gamma := \frac{K_{\|s}}{\widehat{K}_{\|} - \widehat{K}_{\perp}} \ .$$

Then, the introduction of the parameter $K_{\|s}$, related to the mixed contribution of stretch along the cell axis and shear, brings a new parameter γ into the equation for nontrivial equilibrium orientations. As expected, for $\gamma = 0$ we recover the symmetric situation described in Section 3.2.

In order to make some theoretical considerations about stability and bifurcations, the first thing to notice is that if $\gamma \neq 0$ the graph in the (θ, r) plane given by (A.5) presents asymptotes when $\sin 2\theta + 2\gamma\cos 2\theta = 0$, namely if

$$\theta = -\frac{1}{2}\arctan 2\gamma + k\frac{\pi}{2} , \tag{A.6}$$

and it has stationary points when $\tan^3 2\theta = 2\gamma$, i.e. whenever

$$\theta = \frac{1}{2}\arctan \sqrt[3]{2\gamma} + k\frac{\pi}{2}, \tag{A.7}$$

achieving in them a value such that

$$\frac{1}{r+1} = \frac{1}{2}\left(1 \pm \frac{1}{\mathcal{K}\left(1 + \sqrt[3]{4\gamma^2}\right)^{3/2}}\right) \ .$$

Now we discuss the stability of the equilibrium orientations obtained by (A.5). In this case, recalling Eq. (27), the second derivative of the elastic energy can be written in general as

$$U''(\theta) = \varepsilon^2\left\{A\xi'(\theta)^2 + [A\xi(\theta) - B(r+1) + C]\xi''(\theta) + 4K_{\|s}(1-r^2)\sin\theta\cos\theta\right\} .$$

Our goal is to study the sign of this derivative when evaluated in the equilibrium angles: in particular, we can focus on the stability condition given by the inequality

$$A\sin^2 2\theta(1+r) - A(1+r)\cos^2\theta\cos 2\theta + B(1+r)\cos 2\theta - C\cos 2\theta + 2K_{\|s}(1-r)\sin 2\theta > 0.$$

Substituting Eq. (A.5) and dividing by $\cos^2 2\theta$ leads to

$$\frac{1}{\mathcal{K}}\tan^2 2\theta - \frac{1}{\mathcal{K}} + \frac{1}{\mathcal{K}}\frac{\sin 2\theta}{\sin 2\theta + 2\gamma\cos 2\theta}(1 - 2\gamma\tan 2\theta) > 0 \tag{A.8}$$

which is equivalent to

$$\frac{1}{\mathcal{K}}\frac{\tan^3 2\theta - 2\gamma}{\tan 2\theta + 2\gamma} > 0. \tag{A.9}$$
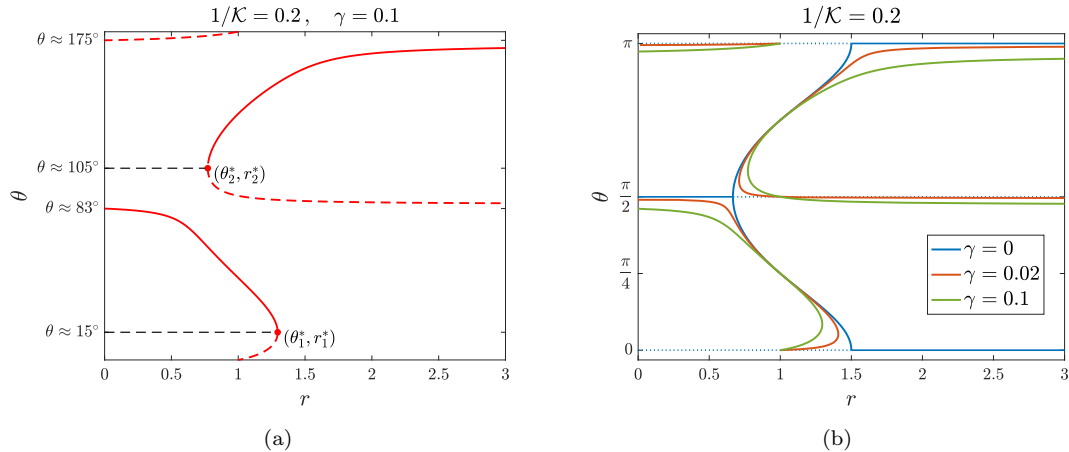
25

Figure 7: (a) Bifurcation diagram in the general case $K_{s\parallel} \neq 0$ for $1/\mathcal{K} = 0.2$, $\gamma = 0.1$. Differently from the symmetric case, here we have two turning points in (θ_1^*, r_1^*) and (θ_2^*, r_2^*). (b) The introduction of γ induces a symmetry breaking in the system, switching from pitchfork to saddle-node bifurcations.

Therefore, if $\mathcal{K} > 0$, the stable configurations are those with

$$\theta \in \left[\frac{1}{2} \arctan \sqrt[3]{2\gamma}, \frac{\pi}{2} - \frac{1}{2} \arctan 2\gamma \right] \cup \left[\frac{\pi}{2} + \frac{1}{2} \arctan \sqrt[3]{2\gamma}, \pi - \frac{1}{2} \arctan 2\gamma \right]. \quad (A.10)$$

Instead, if $\mathcal{K} < 0$, the angles corresponding to stable orientations for the cell are given by

$$\theta \in \left[0, \frac{1}{2} \arctan \sqrt[3]{2\gamma} \right] \cup \left[\frac{\pi}{2} - \frac{1}{2} \arctan 2\gamma, \frac{\pi}{2} + \frac{1}{2} \arctan \sqrt[3]{2\gamma} \right] \cup \left[\pi - \frac{1}{2} \arctan 2\gamma, \pi \right]. \quad (A.11)$$

Then, putting together the information given by the second derivative and the equation of the bifurcation curves, we can draw the bifurcation diagram of the system, shown in Figure 7(a) for the case $\mathcal{K} > 0$. In particular, we observe that for $r < r_2^*$ there are two equilibria, one stable and one unstable; however, when r crosses the critical value r_2^*, two new equilibria appear, of which one is stable and another one is unstable. Finally, we have another visible bifurcation for $r = r_1^*$, when the first two equilibria collide and annihilate each other. In order to give an idea of some numerical values, we reported in the plot in Fig. 7(a) some notable values of θ: more specifically, concerning the peculiar case we considered for $\mathcal{K}$ and γ, i.e. $\gamma = 0.1$ and $\mathcal{K} = 5$, for $r < r_2^*$ we have a stable orientation which is less than $\pi/2$. Variations of γ and $\mathcal{K}$ in $\mathbb{R}^+$ do not alter the qualitative behaviour of the system, but only the shape of the bifurcation diagram (see green and red curve in Fig. 7(b)).

The main difference from the symmetric case treated in Section 3.2 lies in the type of bifurcations involved: here we have two *saddle-node bifurcations*. Then, the introduction of the mixing parameter $K_{\parallel s}$ provokes the disappearance of the pitchfork bifurcations, while two *turning points* appear. The biggest consequence of this fact, which can be observed in Figure 7(b), is that a *symmetry breaking* happens, leading for $\gamma \neq 0$ to equilibrium orientations that are not symmetric. This is due to the fact that the introduction of the coefficient $K_{\parallel s}$ brings into the energy a term proportional to $\sin \theta \cos \theta$, which is neither even nor symmetric with respect to $\pi/2$ as in the previous case. Consequently, unlike the symmetric case, one has $U(-\theta) \neq U(\theta)$ and

26

$U(\pi - \theta) \neq U(\theta)$, but $U(\pi - \theta) = U(-\theta)$. However, this situation is not biologically meaningful, because there is no reason why one of the two orientations corresponding to $-\theta$ or θ should be energetically preferable for the cell with respect to the other, unless one can envisage an internal (left-right) bias in the cell itself. Therefore, we can conclude that, from the biological point of view, in the problem at hand the assumption $K_{\parallel s} = 0$ made in the paper is justified, since we expect to have symmetries in the system which would be broken if this coefficient is not null.

Acknowledgments

Declaration of Competing Interests

The authors declare that they have no known competing financial interests or personal relationships that could have appeared to influence the work reported in this paper.

References

[1] S. Asano, S. Ito, M. Morosawa, K. Furuya, K. Naruse, M. Sokabe, E. Yamaguchi, Y. Hasegawa. Cyclic stretch enhances reorientation and differentiation of 3-D culture model of human airway smooth muscle, *Biochem. Biophys. Rep.* **16**, 32-38 (2018).

[2] G. Astarita, G. Marrucci. Principles of Non-Newtonian Fluid Mechanics, McGraw-Hill (1974).

[3] I.B. Bischofs, U.S. Schwarz. Cell organization in soft media due to active mechanosensing, *Proc. Nat. Acad. Sci. U.S A.* **100**, 9274–9279 (2003).

[4] A.B.C. Buskermolen, H. Suresh, S.S. Shishvan, A. Vigliotti, A. DeSimone, N.A. Kurniawan, C.V.C. Bouten, V.S. Deshpande. Entropic forces drive cellular contact guidance, *Biophys. J.* **116**, 1994-2008 (2019).

[5] D.T. Butcher, T. Alliston, V.M. Weaver. A tense situation: forcing tumour progression, *Nat. Rev. Cancer* **9**, 108-122 (2009).

[6] J.P. Butler, I.M.Tolić-Nørrelykke, B. Fabry, J.J. Fredberg. Traction fields, moments, and strain energy that cells exert on their surroundings, *Am. J. Physiol.: Cell Physiol.* **282**, C595-C605 (2002).

[7] W. Carver, E.C. Goldsmith. Regulation of tissue fibrosis by the biomechanical environment, *Biomed Res. Int.*, 101979 (2013).

[8] M. Chaplain, L. Graziano, L. Preziosi. Mathematical modelling of the loss of tissue compression responsiveness and its role in solid tumour development, *Math. Med. Biol.*, **23**, 197-229, (2006).

[9] B. Chen, R. Kemkemer, M. Deibler, J. Spatz, H. Gao. Cyclic stretch induces cell reorientation on substrates by destabilizing catch bonds in focal adhesions, *PLoS ONE* **7**, e48346 (2012).

[10] K. Chen, A. Vigliotti, M. Bacca, R.M. McMeeking, V.S. Deshpande, J.W. Holmes. Role of boundary conditions in determining cell alignment in response to stretch *Proc. Nat. Acad. Sci. U.S.A.* **115**, 986-991 (2018).

[11] Y. Chen, A.M. Pasapera, A. P. Koretsky, C.M. Waterman, Orientation-specific responses to sustained uniaxial stretching in focal adhesion growth and turnover. *Proc. Nat. Acad. Sci U.S.A.* **110**, E2352-E2361 (2013).

[12] J. Ciambella, P. Nardinocchi. Torque-induced reorientation in active fibre-reinforced materials, *Soft Matter* **15**, 2081–2091 (2019).

[13] J. Ciambella, P. Nardinocchi. A structurally frame-indifferent model for anisotropic visco-hyperelastic materials, *J. Mech. Phys. Solids* **147**, 104247 (2021).

[14] G. Civelekoglu-Scholey, A. Wayne Orr, I. Novak, J.-J. Meister, M.A. Schwartz, A. Mogilner. Model of coupled transient changes of Rac, Rho, adhesions and stress fibers alignment in endothelial cells responding to shear stress, *J. Theor. Biol.* **232**, 569–585 (2005).

[15] A.M. Collinsworth, C.E. Torgan, S.N. Nagda, R.J. Rajalingam, W.E. Kraus, G.A. Truskey. Orientation and length of mammalian skeletal myocytes in response to a unidirectional stretch, *Cell Tissue Res.* **302**, 243–251 (2000).

[16] P. Costa, F.V.M. Almeida, J. T. Connelly. Biophysical signals controlling cell fate decisions: How do stem cells really feel? *Int. J. Biochem. Cell Biol.* **44**, 2233-2237 (2012).

[17] R. De. A general model of focal adhesion reorientation dynamics in response to static and cyclic stretch, *Commun. Biol.* **1**, 81 (2018).

[18] R. De, A. Zemel, S.A. Safran. Dynamics of cell orientation, *Nat. Phys.* **3**, 655–659 (2007).

[19] R. De, A. Zemel, S.A. Safran. Do cells sense stress or strain? Measurement of cellular orientation can provide a clue, *Biophys. J.* **94**, L29–L31 (2008).

[20] V. Deshpande, A. DeSimone, R. McMeeking, P. Recho. Chemo-mechanical model of a cell as a stochastic active gel, *J. Mech. Phys. Solids* **151**, 104381 (2021).

[21] D.E. Discher, D.J. Mooney, P.W. Zandstra. Growth factors, matrices, and forces combine and control stem cells, *Science* **324**, 1673–1677 (2009).

[22] M. Eastwood, V.C. Mudera, D.A. McGrouther and R.A. Brown. Effect of precise mechanical loading on fibroblast populated collagen lattices: Morphological changes, *Cell. Motil. Cytoskeleton* **40**, 13-21 (1998).

[23] U. Faust, N. Hamp, W. Rubner, N. Kirchgebner, S. Safran, B. Hoffmann, R. Merkel. Cyclic stress at mHz frequencies aligns fibroblasts in direction of zero strain, *PLoS ONE* **6**, e28963 (2011).

[24] E.D. Goley, M.D. Welch. The ARP 2/3 complex: an actin nucleator comes of age, *Nat. Rev. Mol. Cell Biol.* **7**, 713–726 (2006).

[25] Z. Goli-Malekabadi, M. Tafazzoli-Shadpour, M. Rabbani, M. Janmaleki. Effect of uniaxial stretch on morphology and cytoskeleton of human mesenchymal stem cells: Static vs. dynamic loading, *Biomed. Tech.* **56**, 259-265 (2011).

[26] F. Guilak, D.M. Cohen, B.T. Estes, J.M. Gimble, W. Liedtke, C.S. Chen. Control of stem cell fate by phisical interactions the the extracellular matrix, *Cell Stem Cell* **5**, 17–26 (2009).

[27] K. Hayakawa, N. Sato, T. Obinata. Dynamic reorientation of cultured cells and stress fibers under mechanical stress from periodic stretching, *Exp. Cell Res.* **268**, 104–114 (2001).

[28] H.-J. Hsu, C.-F. Lee, R. Kaunas. A dynamic stochastic model of frequency-dependent stress fiber alignment induced by cyclic stretch, *PLoS ONE* **4(3)**, e4853 (2009).

[29] D. Ingber. Mechanobiology and diseases of mechanotransduction, *Annals Medicine* **35**, 1–14 (2009).

[30] S. Jungbauer, H. Gao, J.P. Spatz, R. Kemkemer. Two characteristic regimes in frequency-dependent dynamic reorientation of fibroblasts on cyclically stretched substrates, *Biophys. J.* **95**, 3470–3478 (2008).

[31] R. Kalluri, R.A. Weinberg. The basics of epithelial-mesenchymal transition, *J. Clin. Invest.* **119**, 1420-1428 (2009).

[32] J. Kass, M. Erler, M. Dembo, V.M. Weaver. Mammary epithelial cell: Influence of ECM composition and organization during development and tumorigenesis, *Int. J. Biochem. Cell Biol.* **39**, 1987–1994 (2007).

[33] B.-S. Kim, J. Nikolovski, J. Bonadio, D.J. Mooney. Cyclic mechanical strain regulates the development of engineered smooth muscle tissue, *Nat. Biotechnol.* **17**, 979–983 (1999).

[34] F. Kong, A.J. García, A.P. Mould, M.J. Humphries, C. Zhu, Demonstration of catch bonds between an integrin and its ligand. *J. Cell Biol.* **185**, 1275-1284 (2009)

[35] D. Kong, B. Ji, L. Dai. Stability of adhesion clusters and cell reorientation under lateral cyclic tension, *Biophys. J.* **95**, 4034–4044 (2008).

[36] S. Kumar, V.M. Weaver. Mechanics, malignancy, and metastasis: the force journey of a tumor cell, *Cancer Metastasis Rev.* **28**, 113—127 (2009).

[37] Z. Li, H. Lee, C. Zhu. Molecular mechanisms of mechanotransduction in integrin-mediated cell-matrix adhesion *Exp. Cell Res.* **349**, 85–94 (2016).

[38] B. Liu, M.-J. Qu, K.-R. Qin, H. Li, Z.-K. Li, B.-R. Shen, Z.-R. Jiang. Role of cyclic strain frequency in regulating the alignment of vascular smooth muscle cells in vitro, *Biophys. J.* **94**, 1497-1507 (2008).

[39] C. Liu, S. Baek, J. Kim, E. Vasko, R. Pyne, C. Chan. Effect of static pre-stretch induced surface anisotropy on orientation of mesenchymal stem cells, *Cell Mol. Bioeng.* **7**, 106-121 (2014).

[40] A. Livne, E. Bouchbinder, B. Geiger. Cell reorientation under cyclic stretching, *Nat. Comm.* **5**, 3938 (2014).

[41] L. Lu, S.J. Oswald, H. Ngu, F. C.-P. Yin. Mechanical properties of actin stress fibers in living cells, *Biophys. J.* **95**, 6060–6071 (2008).

[42] G. Lucci, L. Preziosi. A nonlinear elastic description of cell preferential orientations over a stretched substrate, *Biomech. Model. Mechanobiol.* **20**, 631–649 (2021).

[43] T. Mao, Y. He, Y. Gu, Y. Yang, Y. Yu, X. Wang, J. Ding. Critical Frequency and Critical Stretching Rate for Reorientation of Cells on a Cyclically Stretched Polymer in a Microfluidic Chip, *ACS Appl. Mater. Interfaces* **13**, 13934-13948 (2021).

[44] A.B. Mathur, W.M. Reichert, G.A. Truskey. Flow and high affinity binding affect the elastic modulus of the nucleus, cell body and the stress fibers of endothelial cells, *Ann. Biomed. Eng.* **35**, 1120–1130 (2007).

[45] M. Moretti, A. Prina-Mello, A.J. Reid, V. Barron, P. J. Prendergast. Endothelial cell alignment on cyclically-stretched silicone surfaces, *J. Mater. Sci.: Mater. in Med.* **15**, 1159—1164 (2004).

[46] M. Morioka, H. Parameswaran, K. Naruse, M. Kondo, M. Sokabe, Y. Hasegawa, B. Suki, S. Ito. Microtubule dynamics regulate cyclic stretch-induced cell alignment in human airway smooth muscle cells, *PLoS ONE* **6**, e26384 (2011).

[47] C. Neidlinger-Wilke, E.S. Grood, J.H.-C. Wang, R.A. Brand, L. Claes. Cell alignment is induced by cyclic changes in cell length: studies of cells grown in cyclically stretched substrates, *J. Orthop. Res.* **19**, 286–293 (2001).

[48] C. Neidlinger-Wilke, E. Grood, L. Claes, R. Brand. Fibroblast orientation to stretch begins within three hours, *J. Orthop. Res.* **20**, 953–956 (2002).

[49] R.W. Ogden. Nonlinear elasticity, anisotropy, material stability and residual stresses in soft tissue, in **Biomechanics of Soft Tissue in Cardiovascular Systems**, 65–108, G.A. Holzapfel and R.W. Ogden, Eds., Springer (2003).

[50] A. Palamidessi, E. Frittoli, N. Ducano, N. Offenhauser, S. Sigismund, H. Kajiho, D. Parazzoli, A. Oldani, M. Gobbi, G. Serini, P.P. Di Fiore, G. Scita, L. Lanzetti. The GTPase-activating protein RN-3 controls focal adhesion turnover and cell migration, *Current Biol.* **23**, 2355—2364 (2013).

[51] A.M. Pasapera, I.C. Schneider, E. Rericha, D.D. Schlaepfer, C.M. Waterman. Myosin II activity regulates vinculin recruitment to focal adhesions through FAK-mediated paxillin phosphorylation, *J. Cell Biol.* **188**, 877—890 (2010).

[52] H.E. Pettermann, A. DeSimone. An anisotropic linear thermo-viscoelastic constitutive law, *Mech. Time-Depend. Mater.* **22**, 421–433 (2018).

[53] H.E. Pettermann, C. Cheyrou, A. DeSimone. Modeling and simulation of anisotropic linear viscoelasticity, *Mech. Time-Depend. Mater.* (2020).

[54] L. Preziosi, G. Vitale. A multiphase model of tumour and tissue growth including cell adhesion and plastic re-organisation, *Math. Models Methods Appl. Sci.* **21**, 1901–1932 (2011).

[55] J. Qian, H. Liu, Y. Lin, W. Chen, H. Gao. A mechanochemical model of cell reorientation on substrates under cyclic stretch, *PLoS ONE* **8**, e65864 (2013).

[56] A. Roshanzadeh, T.T. Nguyen, K.D. Nguyen, D.-S. Kim, B.-K. Lee, D.-W. Lee, E.-S. Kim. Mechanoadaptive organization of stress fiber subtypes in epithelial cells under cyclic stretches and stretch release, *Sci. Rep.* **10**, 18684 (2020).

[57] I. Rouiller, X.-P. Xu, K.J. Amann, C. Egile, S. Nickell, D. Nicastro, R. Li, T.D. Pollard, N. Volkmann, D. Hanein. The structural basis of actin filament branching by the Arp2/3 complex, *J. Cell Biol.* **180**, 887–895 (2008).

[58] L.E. Scott, S.H. Weinberg, C.A. Lemmon. Mechanochemical Signaling of the Extracellular Matrix in Epithelial-Mesenchymal Transition, *Front. Cell Dev. Biol.* **7**, 135 (2019).

[59] Y. Sun, C.S. Chen, J. Fu. Forcing stem cells to behave: A biophysical perspective of cellular microenvironment, *Annu. Rev. Biophys.* **41**, 519–542 (2012).

[60] L.A. Taber. Biophysical mechanisms of cardiac looping, *Int. J. Dev. Biol.* **50**, 323-332 (2006).

[61] A. Tondon, R. Kaunas. The direction of stretch-induced cell and stress fiber orientation depends on collagen matrix stress, *PLoS ONE* **9**, e89592 (2014).

[62] A. Tondon, H.J. Su, R. Kaunas. Dependence of cyclic stretch-induced stress fiber reorientation on stretch waveform, *J. Biomech.* **45**, 728—735 (2012).

[63] L. Tuan, M.J. Fairchild, J. Michael, A.D., Perkins, G. Tanentzapf. Analysis of integrin turnover in fly myotendinous junctions, *J. Cell Sci.* **123**, 939–946, (2010).

[64] N.L. Tulloch, V. Muskheli, M.V. Razumova, F. Steven Korte, M. Regnier, K.D. Hauch, L. Pabon, H. Reinecke, C.E. Murry. Growth of engineered human myocardium with mechanical loading and vascular coculture, *Circ. Res.* **109**, 47–49 (2011).

[65] A.-M. Vlaikou, D. Kouroupis, A. Sgourou, G.S. Markopoulos, E. Bagli, M. Markou, Z. Papadopoulou, T. Fotsis, G. Nakos, M.-E. E. Lekka, M. Syrrou. Mechanical stress affects methylation pattern of *GNAS* isoforms and osteogenic differentiation of hAT-MSCs, *Biochim. Biophys. Acta-Mol. Cell Res.* **1864**, 1371–1381 (2017).

[66] J. H.-C. Wang. Substrate deformation determines actin cytoskeleton reorganization: A mathematical modeling and experimental study, *J. Theor. Biol.* **202**, 33—41 (2000).

[67] J. H.-C. Wang, P. Goldschmidt-Clermont, J. Wille, F. C.-P. Yin. Specificity of endothelial cell reorientation in response to cyclic mechanical stretching, *J. Biomech.* **34**, 1563—1572 (2001).

[68] H. Wang, W. Ip, R. Bossy, E.S. Grood. Cell orientation response to cyclically deformed substrates: Experimental validation of a cell model, *J. Biomech.* **28**, 1543–1552 (1995).

[69] S. Wang, D. Lu, Z. Zhang, X. Jia, L. Yang. Effects of mechanical stretching on the morphology of extracellular polymers and the mRNA expression of collagens and small leucine-rich repeat proteoglycans in vaginal fibroblasts from women with pelvic organ prolapse, *PLoS ONE* **13**, e0193456 (2018).

[70] Z. Wei, V.S. Deshpande, R.M. McMeeking, A.G. Evans. Analysis and interpretation of stress fiber organization in cells subject to cyclic stretch, *J. Biomech. Eng.-Trans. ASME* **130**, 031009-1 – 031009-9 (2008).

[71] G. Xu, B. Li, X. Feng, H. Gao. A tensegrity model of cell reorientation on cyclically stretched substrates, *Biophys. J.* **111**, 1478–1486 (2016).

[72] F.J. Vernerey, U. Akalp. Role of catch bonds in actomyosin mechanics and cell mechanosensitivity *Phys. Rev. E* **94**, 012403 (2016)

31

[73] Y. Yan, S. Sart, Y. Li. Differentiation of neural progenitor cells from pluripotent stem cells in artificial niches, *Int. J. Stem Cell Res. Transpl.* **1**, 22–27 (2013).

[74] J.-K. Yoon, T. Lee, S.H. Bhang, J.-Y. Shin, J.-M. Myoung, B.-S. Kim. Stretchable piezo-electric substrate providing pulsatile mechanoelectric cues for cardiomyogenic differentiation of mesenchymal stem cells, *ACS Appl. Mater. Interfaces* **9**, 22101–22111 (2017).

[75] C. Zhu. Mechanochemistry: A molecular biomechanics view of mechanosensing, *Ann. Biomed. Engng.* **42**, 388-404 (2014).

[76] C. Zhu, Y. Chen, L.A. Ju. Dynamic bonds and their roles in mechanosensing, *Curr. Opin. Chem. Biol.* **53**, 88-97 (2019).